The N-DRC forms a conserved biochemical complex that maintains outer doublet alignment and limits microtubule sliding in motile axonemes

Raqual Bower[a], Douglas Tritschler[a], Kristyn VanderWaal[a], Catherine A. Perrone[a], Joshua Mueller[a], Laura Fox[b], Winfield S. Sale[b], and M. E. Porter[a]
[a]Department of Genetics, Cell Biology, and Development, University of Minnesota, Minneapolis, MN 55455;
[b]Department of Cell Biology, Emory University School of Medicine, Atlanta, GA 30322

ABSTRACT **The nexin–dynein regulatory complex (N-DRC) is proposed to coordinate dynein arm activity and interconnect doublet microtubules. Here we identify a conserved region in DRC4 critical for assembly of the N-DRC into the axoneme. At least 10 subunits associate with DRC4 to form a discrete complex distinct from other axonemal substructures. Transformation of *drc4* mutants with epitope-tagged DRC4 rescues the motility defects and restores assembly of missing DRC subunits and associated inner-arm dyneins. Four new DRC subunits contain calcium-signaling motifs and/or AAA domains and are nearly ubiquitous in species with motile cilia. However, *drc* mutants are motile and maintain the 9 + 2 organization of the axoneme. To evaluate the function of the N-DRC, we analyzed ATP-induced reactivation of isolated axonemes. Rather than the reactivated bending observed with wild-type axonemes, ATP addition to *drc*-mutant axonemes resulted in splaying of doublets in the distal region, followed by oscillatory bending between pairs of doublets. Thus the N-DRC provides some but not all of the resistance to microtubule sliding and helps to maintain optimal alignment of doublets for productive flagellar motility. These findings provide new insights into the mechanisms that regulate motility and further highlight the importance of the proximal region of the axoneme in generating flagellar bending.**

Monitoring Editor
Erika Holzbaur
University of Pennsylvania

Received: Nov 13, 2012
Revised: Feb 1, 2013
Accepted: Feb 8, 2013

INTRODUCTION

Cilia and flagella are highly conserved, microtubule-based organelles that extend from the surfaces of eukaryotic cells and play critical roles in cell signaling and motility. Defects in components involved in ciliary assembly, signaling, or motility have profound consequences for an organism, and in humans they can lead to a wide variety of diseases collectively known as ciliopathies (Hildebrandt *et al.*, 2011; Drummond, 2012). Defects in motility are often associated with chronic respiratory disease (primary ciliary dyskinesia [PCD]), male sterility, hydrocephalus, and defects in the development of the left–right body axis (Fliegauf *et al.*, 2007; Lee, 2011; Zariwala *et al.*, 2011). Given that >400 proteins have been identified by both genomic and proteomic strategies as components of the ciliary and flagellar proteome but less than half have been clearly correlated with a specific structure or function (Li *et al.*, 2004; Pazour *et al.*, 2005; Ishikawa *et al.*, 2012; Mizuno *et al.*, 2012), there is considerable interest in a more comprehensive definition of axoneme substructures, including conserved protein complexes required for regulation of motility.

Most motile cilia and flagella contain a structure known as the 9 + 2 axoneme, which consists of nine outer doublet microtubules arranged in a ring surrounding a central pair (CP) of two singlet microtubules. The outer and inner dynein arms (ODA and IDA, respectively) are the motor enzymes that drive ciliary motility, and they are arranged in two distinct rows along the length of the A-tubule of each outer doublet. The motor domains of the dyneins walk along

This article was published online ahead of print in MBoC in Press (http://www.molbiolcell.org/cgi/doi/10.1091/mbc.E12-11-0801) on February 20, 2013.

Address correspondence to: Mary E. Porter (porte001@umn.edu).

Abbreviations used: CP, central pair; CSC, calmodulin spoke complex; DHC, dynein heavy chain; DRC, dynein regulatory complex; FAP, flagellar associated polypeptide; GFP, green fluorescent protein; IDA, inner dynein arm; iTRAQ, isobaric tag for relative and absolute quantitation; MS, mass spectrometry; N-DRC, nexin–dynein regulatory complex; ODA, outer dynein arm; PCD, primary ciliary dyskinesia; PF, paralyzed flagella; RS, radial spoke; WT, wild type.

the surface of the B-tubule of the neighboring doublet in an ATP-sensitive manner and thereby generate sliding forces between the doublet microtubules. Because the outer doublets are attached to basal bodies at their base and cross-linked by nexin linkages every 96 nm along their length, microtubule sliding between the doublets is constrained and converted into axonemal bending. In addition, both the ODAs and IDAs are minus end–directed motors that push adjacent doublets toward the tip of the axoneme during bending (Sale and Satir, 1977; Fox and Sale, 1987). Dynein cross-bridge activity must therefore be switched on and off on opposite sides of the axoneme for effective bending to occur (Wais-Steider and Satir, 1979; Satir and Matsuoka, 1989; Brokaw, 2009a).

Three distinct but overlapping models have been proposed for how dynein activity might be regulated during the ciliary beat cycle (Brokaw, 2009a; Lindemann and Lesich, 2010; Lindemann, 2011; Porter, 2012). One model (the sliding control model) suggests that the basic mechanics of the dynein cross-bridge cycle coupled with the linear arrangement of dynein motors along the length of the outer doublets results in the sequential activation and termination of dynein activity during bending (Riedel-Kruse *et al.*, 2007; Brokaw, 2009a; Lindemann and Lesich, 2010; Mitchison and Mitchison, 2010). Another view is that ciliary bending alters the activity of dynein cross-bridges by changes in doublet curvature or doublet spacing (curvature control or geometric clutch models; Morita and Shingyoji, 2004; Hayashi and Shingyoji, 2008; Lindemann and Mitchell, 2007; Lindemann and Lesich, 2010; Brokaw, 2009a). These changes increase or decrease the probability that a dynein arm can form a cross-bridge with a neighboring doublet. Both of these models are influenced by factors that affect the affinity of the dynein cross-bridges and/or the behavior of the nexin linkages.

A third view is that dynein activity is modulated by a series of mechanical and enzymatic interactions that involve the CP microtubules and their associated projections, the radial spokes (RSs), the calmodulin spoke complex (CSC), and the dynein regulatory complex (DRC). This model (the distributor model) is based on the need for additional mechanisms to modify dynein activity in response to intracellular and extracellular signals (e.g., calcium) and also on a large body of work with *Chlamydomonas* flagellar mutants (Porter and Sale, 2000; Porter, 2012; Smith and Yang, 2004). The model proposes that the CP projections make contacts with the radial spokes in an asymmetric manner during axonemal bending. Differences in strain or tension are transduced through the RS to the CSC, the DRC, and/or other, unidentified components to inhibit or activate different subsets of inner dynein arms. The detailed mechanism is not clear, but pharmacological studies indicate that several tightly bound axonemal kinases and phosphatases may also be involved in regulating the velocity of dynein-driven sliding (Porter and Sale, 2000; Wirschell *et al.*, 2011).

Although these three models reflect different perspectives on the various mechanisms that regulate dynein activity, all three models require some component within the axoneme that limits dynein activity and the extent of microtubule sliding (Brokaw, 2009a; Lindemann and Lesich, 2010; Woolley, 2010; Porter, 2012). In the distributor model, this component is the DRC, because mutations in the DRC can override the paralysis observed with CP and RS mutations and restore some form of flagellar motility. Mutations in the DRC are also associated with defects in the assembly of a subset of tightly bound axonemal polypeptides (Huang *et al.*, 1982; Piperno *et al.*, 1992, 1994) that have been correlated with defects in the assembly of a large structure at the distal end of the 96-nm axoneme repeat, between RS2 and the dynein arms (Supplemental Table S1; Mastronarde *et al.*, 1992; Gardner *et al.*, 1994). Reexamination of the *drc* mutants by cryo–electron tomography (cryo-ET) demonstrated that the DRC is an integral part of the nexin link, now referred to as the nexin–dynein regulatory complex (N-DRC; Heuser *et al.*, 2009). Both improvements in resolution and the ability to view the N-DRC in three dimensions have further revealed numerous connections between the N-DRC and other structures, such as the ODAs, IDAs, RS2, and CSC (Heuser *et al.*, 2009, 2012a,b; Pigino *et al.*, 2011, 2012; Barber *et al.*, 2012; Bui *et al.*, 2012). As a result, there is considerable interest in defining the different subunits of the DRC and their interactions with other axonemal complexes (Lin *et al.*, 2011; Heuser *et al.*, 2012a).

In this study, we used DRC4 and associated mutations as a starting point to reanalyze the biochemical composition of the N-DRC, identify subcomplexes with the N-DRC, and further test the role of the N-DRC in regulating microtubule sliding. We previously showed that the *PF2* gene product, DRC4, is the *Chlamydomonas* orthologue of a highly conserved coiled-coil protein known as Gas11 in humans, Gas8 in other vertebrates, and trypanin in trypanosomes (Rupp and Porter, 2003; Ralston and Hill, 2006; Colantonio *et al.*, 2009). Here we identify a conserved DRC4 region missing in *sup-pf3* that is critical for the assembly of the N-DRC linker. We also used coimmunoprecipitation, iTRAQ labeling, and quantitative mass spectrometry to identify additional N-DRC subunits beyond those previously described by two-dimensional (2D) gel-based methods (Piperno *et al.*, 1992, 1994; Lin *et al.*, 2011). Spectral counting was used to more rigorously define the IDA isoforms most closely associated with the N-DRC. In addition, we generated and characterized several new antibodies and epitope-tagged strains for the analysis of N-DRC in vitro and in vivo. This work shows that the N-DRC behaves as a discrete biochemical complex, distinct from other substructures within the axoneme such as the RS, CSC, and protofilament ribbon. Finally, we used ATP-induced reactivation and microtubule-sliding assays to demonstrate that the N-DRC provides some but not all of the resistance to microtubule sliding and also serves to maintain alignment between outer doublet microtubules during flagellar bending.

RESULTS

Distribution of DRC4 in *drc* mutants

We previously identified the *PF2* gene product as a highly conserved orthologue of the vertebrate protein GAS8/GAS11 that corresponds to a spot on 2D gels known as DRC4 (Rupp and Porter, 2003). To further characterize the properties and distribution of DRC4, we generated polyclonal antibodies against a conserved peptide sequence, EERHQVEIKVYKQKKVKHLLYEH, and a GAS8 fusion protein and tested the affinity-purified antibodies on Western blots of axonemes. Both antibodies recognized an ~50-kDa polypeptide that is present in wild type (WT), missing in *pf2*, and shifted ~5 kDa in the *PF2-HA* rescued sample (Supplemental Figure S1A), thereby demonstrating their specificity for DRC4. The affinity-purified antibodies were then used to probe blots of axonemes isolated from a series of motility mutants (Figure 1A and Supplemental Table S1). DRC4 is present at WT levels in mutants affecting the assembly of the ODAs (*pf28, sup-pf2*) and IDAs (*pf9, ida4*) but is altered to various degrees in *drc* mutants. DRC4 is present in *pf3* and *sup-pf4* but migrates as two smaller bands in *sup-pf3* (Figure 1A). These results are consistent with previous studies using 2D gels: the loss of the WT DRC4 spot in *sup-pf3* correlated with the appearance of two smaller spots (Huang *et al.*, 1982; Lin *et al.*, 2011). Collectively these observations suggested that *sup-pf3* might be an unusual *PF2* mutation that results in modification of DRC4.

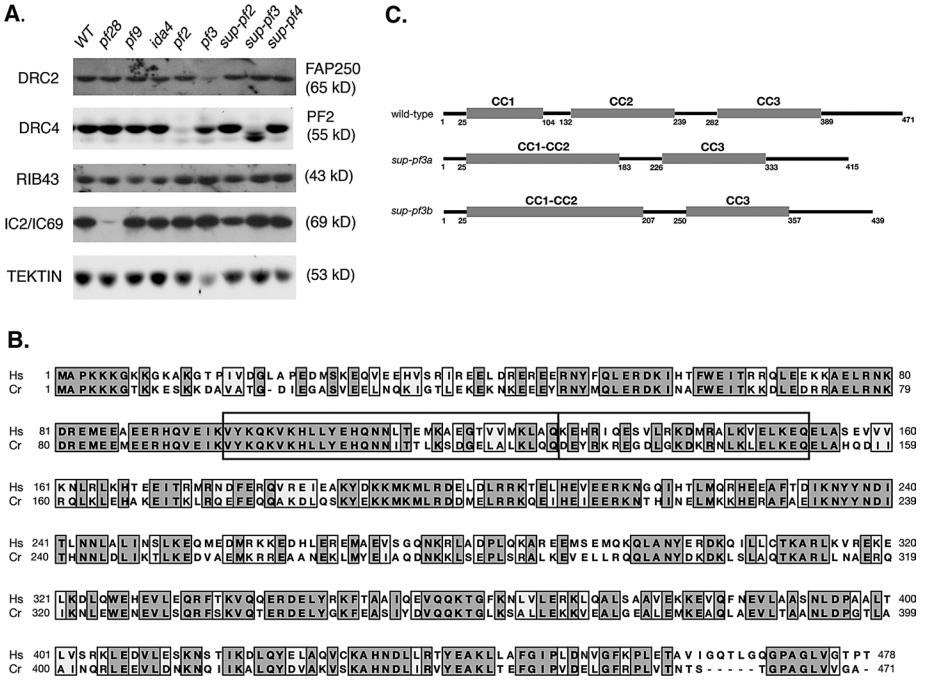

FIGURE 1: DRC4 is truncated by alternative splicing in *sup-pf3*. (A) Western blot of WT and mutant axonemes probed with antibodies to DRC4 reveals the presence of truncated DRC4 subunits in *sup-pf3*. Anti-Rib43 serves as a loading control. The outer-arm subunit IC2 is reduced in the outer-arm mutants *pf28* and *sup-pf2*. DRC2 and tektin are reduced only in *pf3*. (B) Clustal W alignment of the human GAS11 and *Chlamydomonas* DRC4 polypeptide sequences. The deleted amino acids (outlined in the black box) correspond to a region that is highly conserved between DRC4 orthologues. (C) Predicted structural domains in WT and *sup-pf3* DRC4 subunits. The deleted regions are predicted to alter the arrangement of coiled-coil domains 1 and 2 in DRC4.

The *sup-pf3* mutation is caused by insertion of a transposable element in the *PF2* gene

To assess how the *sup-pf3* mutation might affect the *PF2* gene, we amplified 500– to 1000–base pair fragments by PCR from WT and *sup-pf3* genomic DNA and sequenced directly (Supplemental Table S2). No sequence differences were observed, with the exception that we were unable to amplify one small region of the *PF2* gene in *sup-pf3*. We therefore compared *Sac*I digests of WT and *sup-pf3* genomic DNA on Southern blots probed with *PF2* subclones, including an ~1.2-kb *Nhe*I restriction fragment corresponding to nucleotides 2146–3362 (Supplemental Figure S2A). This probe hybridized to 701– and 755–base pair *Sac*I fragments in WT DNA, but the 701–base pair band was shifted to ~7 kb in *sup-pf3* genomic DNA (Supplemental Figure S2B). The shift of the 701–base pair fragment indicated that a major rearrangement had occurred in the region between nucleotides 2744 and 3445.

To characterize the mutation, we constructed a size-fractionated minilibrary from *sup-pf3* genomic DNA and isolated an ~7-kb *Sac*I subclone containing the modified region of *PF2* gene. Sequence analysis revealed the insertion of a large (>5.6 kb) *TOC1* transposable element (Day and Rochaix, 1991) just downstream of the splice acceptor site for exon 4 (Supplemental Figure S2C). To assess how *TOC1* might affect splicing of the *PF2* transcript, we used primers from exons 1 and 5 to amplify reverse transcription PCR (RT-PCR) products from WT and *sup-pf3* cDNA (Supplemental Figure S2D). A 495–base pair RT-PCR product was recovered from control cDNA, but only two smaller products were recovered from *sup-pf3* cDNA (Supplemental Figure S2E). Direct sequencing indicated a deletion of 168 nucleotides in the smaller product (*sup-pf3* splice form A) and a deletion of 96 nucleotides in the larger product (*sup-pf3* splice form B). All of exon 4 was missing in splice form A, whereas splice form B used a cryptic splice site downstream of the *TOC1* insertion site, at nucleotides 3384–3391 of the original exon 4 (Supplemental Figure S2D). The DRC4 subunits encoded by the two novel transcripts contain in-frame deletions of 56 and 32 amino acids, respectively (Figure 1B). The *sup-pf3* splice A product deletes amino acids 96–151 and has a predicted molecular weight of 48.4 kDa and pI of 6.02. The splice B product deletes amino acids 96–127 and has a predicted molecular weight of 51.3 kDa and a pI of 6.18. These changes are consistent with the shifts seen on Western blots (Figure 1A) and 2D gels (Huang *et al.*, 1982; Lin *et al.*, 2011).

The *sup-pf3* mutation deletes a conserved region of the DRC4 subunit

DRC4 is a highly conserved, coiled-coil protein with significant degree of sequence and structural similarity across diverse organisms that assemble motile cilia (Figure 1B; Rupp and Porter, 2003). Exon 4 encodes amino acid residues 96–151, which overlaps with the end of the first predicted coiled-coil domain, CC1 (residues 25–104) and the beginning of the second coiled-coil domain, CC2 (residues 132–239; Figure 1C). CC1 and CC2 have been described as a region mediating an interaction between the mouse GAS8 subunit and Rab3B in vitro (Nishimura *et al.*, 2008), whereas the region containing CC2 has been proposed as a potential microtubule-binding site (GMAD, residues 118–260) in human GAS11 (Hill *et al.*, 2000; Bekker *et al.*, 2007). Deletion of exon 4 might be expected to have a significant impact on DRC4 assembly and function. Analysis of the modified polypeptide sequences predicts that the truncated region could form a contiguous coiled coil (CC1-CC2; Figure 1C).

Rescue of *pf2* and *sup-pf3* by transformation with PF2–green fluorescent protein

Dikaryon rescue experiments previously showed that motility defects in *pf2* could be rescued by mating to WT cells, but rescue of *sup-pf3* required deflagellation and reassembly of new flagella (Huang *et al.*, 1982). These observations suggested that the *sup-pf3* subunits do not readily exchange with their WT counterparts in intact flagella but that *sup-pf3* is recessive to WT after turnover of flagellar proteins after regeneration. To test this hypothesis directly, we transformed *pf2* and *sup-pf3* cells with a green fluorescent protein (GFP)–tagged version of the *PF2* gene, screened GFP-positive cells for rescue of motility, and then analyzed isolated axonemes on Western blots (Figure 2).

Live-cell imaging or immunofluorescence with a GFP antibody revealed DRC4-GFP signal along the length of both flagella and at two spots at the anterior end of the cell, near the basal body region, in rescued strains but not in mutant cells (Figure 2, A and B). As measured by phase contrast microscopy, the forward swimming velocities of the GFP-positive strains were significantly increased relative to either *sup-pf3* or *pf2*, demonstrating that the *PF2-GFP*

transgene is functional with respect to flagellar motility (Figure 2C). However, the swimming velocities of the GFP rescued strains were slightly slower than those in WT cells. These results could indicate that expression from the *PF2-GFP* transgene is reduced relative to that from the endogenous *PF2* gene.

To assess the extent of DRC4-GFP assembly, we analyzed axonemes from WT, mutant, and rescued cells on Western blots. Both the affinity-purified DRC4 antibody and the GFP antibody recognized an ~75-kDa DRC4-GFP band in the *pf2::PF2-GFP* rescued strain (Figure 2D). However, the *sup-pf3::PF2-GFP* strains contained three bands recognized by the DRC4 antibody: a major band corresponding to DRC4-GFP and minor bands corresponding to the modified DRC4 subunits in *sup-pf3* (Figure 2D). Thus DRC4-GFP assembles into the axoneme more efficiently than the truncated *sup-pf3* DRC4 subunits, but it does not completely displace them. The phenotype of truncated *sup-pf3* polypeptides appears to be codominant in the *PF2-GFP* rescued strains. Backcrossing *pf2::PF2-GFP* rescued cells to WT cells confirmed that DRC4-GFP subunits assemble into axonemes at approximately the same stoichiometry as the endogenous WT DRC4 subunits (Bower and Porter, unpublished results). Collectively, the results demonstrate that the *PF2-GFP* transgene can rescue motility in both *pf2* and *sup-pf3* and that DRC4-GFP assembles into flagella at near-WT levels.

Turnover of DRC4 subunits in dikaryon flagella

Flagellar assembly and maintenance require the continuous delivery of precursors to the tips of the flagella by intraflagellar transport before assembly into the axoneme (Qin *et al.*, 2004; Hou *et al.*, 2007; Ahmed *et al.*, 2008). However, earlier efforts to rescue *sup-pf3* mutants by mating to WT cells failed unless the flagella were amputated and allowed to regenerate (Huang *et al.*, 1982). To better understand the process of DRC assembly, we mated *pf2::PF2-GFP* strains to both *pf2* and WT cells and analyzed quadriflagellate dikaryons for the appearance of DRC4-GFP in the unlabeled flagella. Cells of opposite mating type were mixed together, fixed at specific time points, and then processed for immunofluorescence. When *pf2::PF2-GFP* cells were mated to a WT strain, DRC4-GFP signal was clearly visible in the two flagella derived from the *pf2::PF2-GFP* parent (Figure 2E). However, no DRC4-GFP signal was detected in flagella derived from the WT parent, even if the dikaryons were fixed at 10, 30, or 60 min after mixing. These results indicated that there was little exchange between the donor DRC4-GFP subunits and the endogenous, unlabeled DRC4 subunits in WT flagella during the first hour. In contrast, if *pf2::PF2-GFP* cells were mated to *pf2* cells, DRC4-GFP signal could be detected at the tips of the two mutant flagella in <10 min (Figure 2F). DRC4-GFP staining was more evident at 30 min, and by 60 min, DRC4-GFP labeling of the *pf2* flagella had clearly extended proximally, toward the cell body (Figure 2F). This pattern of initial staining at the flagellar tip followed by the spread of the signal proximally toward the flagellar base is similar to the pattern described previously for the assembly of radial spokes in WT × *pf14* dikaryons (Johnson and Rosenbaum, 1992).

Reassembly of inner-arm dyneins in PF2-rescued strains

Several studies identified deficiencies in assembly of single-headed, IDA isoforms in *pf2* and *sup-pf3* axonemes, especially dynein *e* (Piperno *et al.*, 1992, 1994; Gardner *et al.*, 1994; Supplemental Table S1). These deficiencies have been correlated with defects in inner arm structures closely associated with the N-DRC (Gardner *et al.*, 1994; Rupp and Porter, 2003; Bui *et al.*, 2009; Heuser *et al.*, 2009). Moreover, rescue of *pf2* with either the *PF2-HA* or *PF2-GFP* transgene resulted in the reassembly of the missing IDA structures (Rupp and Porter, 2003; Heuser *et al.*, 2009). However, the complexity of dynein heavy chain (DHC) composition in *Chlamydomonas* axonemes (Porter *et al.*, 1996; Yagi *et al.*, 2009; Bui *et al.*, 2012) has made a clear description of the specific DHC defects difficult. In addition, some DHCs are more resistant to high salt extraction than others (Pazour *et al.*, 2005; Yagi *et al.*, 2009), and so analysis of dynein extracts can be potentially misleading.

As an alternative strategy for the identification of dynein defects in the *drc* mutants, we used spectral counting (Zhu *et al.*, 2010) to quantify inner-arm DHCs in isolated axonemes. Axonemes from WT, *pf2*, and *pf2::PF2-HA* rescued strains were separated by SDS–PAGE, and the DHC region was excised from the gels. Each sample was extracted and trypsin digested, and then three to five replicates per sample were analyzed by tandem mass spectrometry (MS/MS). Both the total number of unique peptides and the total number of assigned spectra per DHC subspecies were analyzed. Because assembly of the I1 dynein is largely unaffected in *pf2* mutants (Mastronarde *et al.*, 1992; Gardner *et al.*, 1994), the total number of assigned spectra for each DHC was normalized to the total number of assigned spectra for the 1-α and 1-β DHCs of the I1 dynein. As shown in Figure 3A, assembly of DHC8 was significantly reduced ($p < 0.005$) in *pf2* relative to both the WT and the *pf2::PF2-HA* strain. We also detected a slight but statistically significant decrease ($p < 0.005$) in DHC2 in *pf2* relative to both WT and *pf2::PF2-HA*. The observed changes in the relative abundance of other inner-arm DHCs in *pf2,* including DHC5, were not statistically significant when compared with both WT and *pf2::PF2-HA* rescued strains. Western blots of WT and *pf2* axonemes probed with antibodies against several dynein subunits confirmed that most of the other dynein subspecies were not significantly reduced in *pf2* (Figure 3B). We conclude that dynein *e* (DHC8) is the major inner-arm subspecies whose assembly is disrupted in *pf2*, consistent with our previous analysis of *pf2* and *sup-pf3* dynein extracts by fast-performance liquid chromatography (FPLC; Gardner *et al.,* 1994), and that the recovery of DHC8 correlates with the reassembly of IA4 in the rescued strains (Rupp and Porter, 2003; Heuser *et al.,* 2009).

Interactions between DRC4, the RS, the CSC, and the protofilament ribbon

To identify other polypeptides closely associated with DRC4, we extracted isolated flagella with different buffers to define conditions that release DRC4 from the axoneme. Flagellar components involved in intraflagellar transport (IFT) are typically extracted by treatment with nonionic detergents and/or high concentrations of MgATP (Cole *et al.*, 1998), whereas most of the inner and outer dynein arms are released by treatment with 0.6 M NaCl (Piperno and Luck, 1979). In contrast, extraction of the central pair (CP) and RS complexes usually requires treatment with 0.2–0.6 M NaI (Mitchell and Sale, 1999; Yang *et al.*, 2001). Very little DRC4 was released after extraction with nonionic detergents, 10 mM ATP, or 0.5 M NaCl, but significant quantities of DRC4 were released by extraction of axonemes with 0.5 M NaI (Supplemental Figure S3A). Because both structural and biochemical studies have shown that the N-DRC is closely associated with radial spoke 2 (RS2) and components of a calmodulin spoke–associated complex (CSC; Mastronarde *et al.*, 1992; Gardner *et al.*, 1994; Piperno, 1995; Rupp and Porter, 2003; Heuser *et al.*, 2009, 2012a; Dymek *et al.*, 2011), we also analyzed extraction of the N-DRC in the RS mutant *pf14* and extraction of the RS and CSC in the *pf2* mutant. High-salt treatment of *pf14* axonemes released the CSC subunit CaM-IP3 (flagellar associated polypeptide 61 [FAP61]) at relatively low ionic strength, but extraction of DRC4 was unaffected by the absence of the RS (Supplemental Figure S3B).

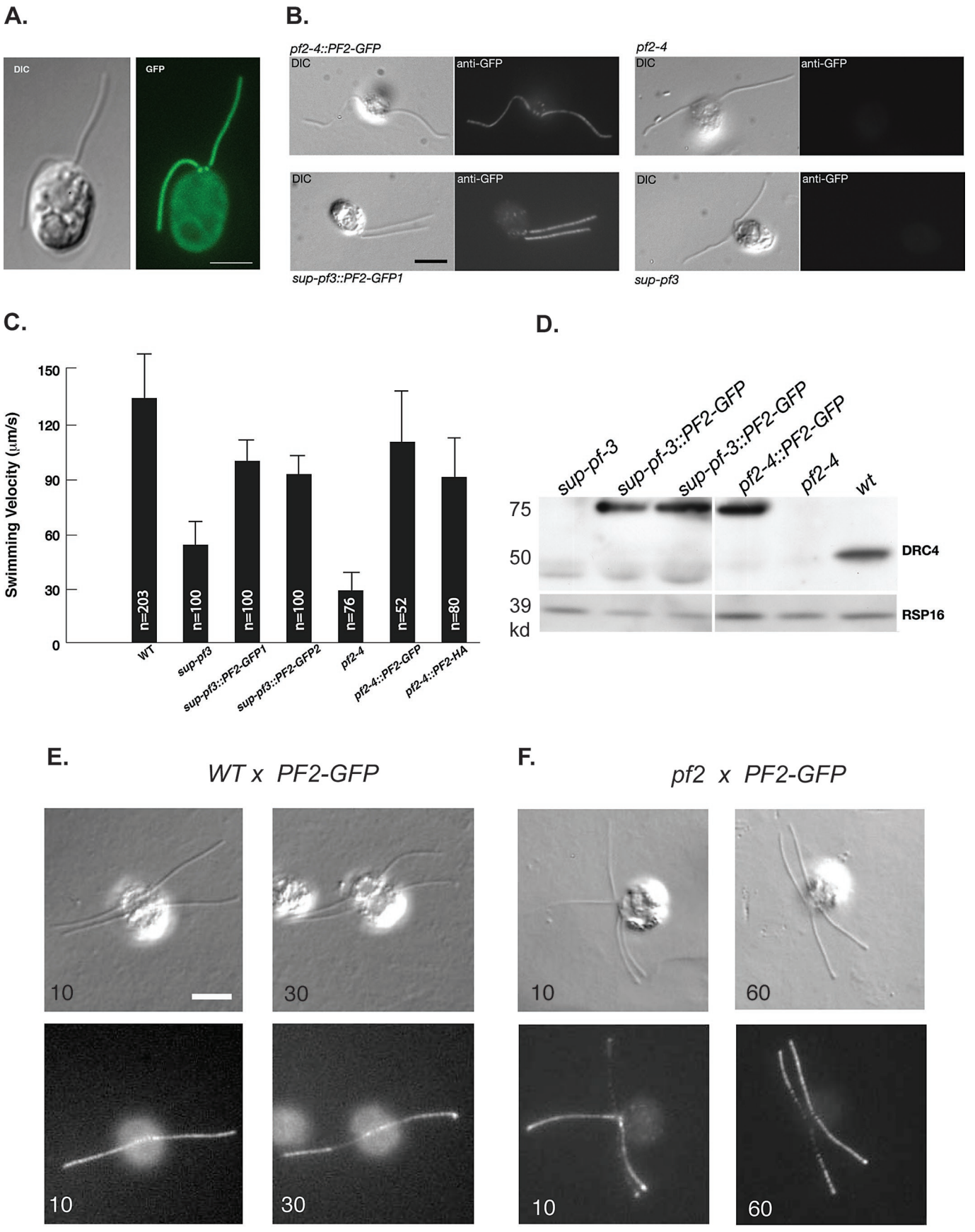

FIGURE 2: *PF2-GFP* rescues the mutant phenotypes associated with *pf2* and *sup-pf3*. (A) Live imaging of an immobilized *PF2-GFP* rescued cell by DIC and fluorescence microscopy reveals that DRC4-GFP is located near the basal body region and along the length of the flagella. (B) DIC and fluorescence imaging of fixed *PF2-GFP* rescued cells (left)

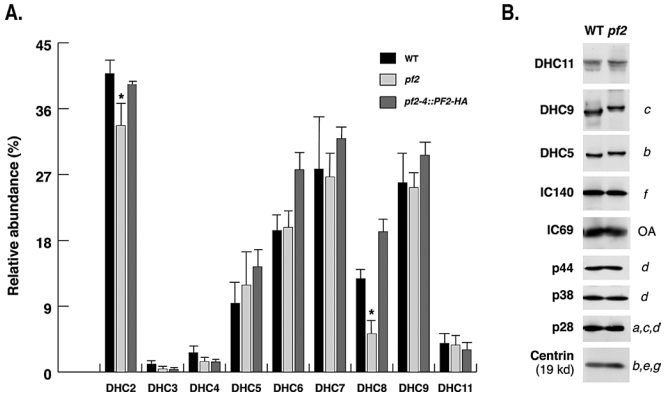

FIGURE 3: Inner-arm dynein subspecies in *pf2*. (A) Isolated axonemes from WT, *pf2-4*, and *pf2-4::PF2-HA* were separated on a 5% SDS–PAGE gel, the DHC regions were excised, and three to five replicates were analyzed by MS/MS and spectral counting. The total number of spectra for each DHC subspecies was expressed as a percentage of the total number of spectra for the two DHCs of the I1 dynein. DHC8 was substantially reduced in *pf2*, and DHC2 was slightly reduced (p <0.005). (B) Western blot of WT and *pf2* axonemes probed with antibodies against various dynein subunits. No obvious defects were observed with antibodies against the outer-arm (OA) subunit IC69 or the inner-arm subunits shown here. No antibodies were available for DHC2 or DHC8.

In contrast, both RSP16 and CaM-IP3 required extraction with 0.4–0.6 M NaI in the *pf2* mutant (Supplemental Figure S3C). The extraction profiles are consistent with the close physical interaction between RS2 and the CSC (Dymek and Smith, 2007; Dymek *et al.*, 2011; Heuser *et al.*, 2012a) but also suggest that DRC4 is part of a distinct complex.

The extraction of DRC4 by 0.4–0.6 M NaI implies that the N-DRC is tightly bound to the surface of the microtubule but not an integral component of the underlying outer doublet. This prediction is consistent with observation that *pf2* axonemes lacked the linker region of the N-DRC but the outer doublet microtubules appeared unaltered when viewed in cross section or by cryo-ET (Mastronarde *et al.*, 1992; Gardner *et al.*, 1994; Rupp and Porter, 2003; Heuser *et al.*, 2009). However, this region has also been proposed as binding site of several proteins (Rib72, PACRG) associated with the protofilament ribbon that might contribute to the periodic spacing and assembly of the N-DRC (Ikeda *et al.*, 2003, 2007). In addition, the surface of the outer doublet microtubules was altered in the *drc* mutant *pf3* (Heuser *et al.*, 2009). To determine whether there might be any interaction between DRC4 and subunits of the protofilament ribbon, we probed Western blots of *drc* mutant axonemes with antibodies against ribbon subunits. However, we observed no evidence for a significant change in the levels of either Rib43 (Figure 1A) or Rib72 (Wirschell *et al.*, 2013; Bower and Porter, unpublished results) in any of the *drc* mutants. To test whether DRC4 might remain bound to the ribbon during sarkosyl extraction, we analyzed WT axonemes and ribbon fractions on Western blots. Rib43 and Rib72 were quantitatively retained in the ribbon fraction after sarkosyl extraction, as previously described (Norrander *et al.*, 2000; Ikeda *et al.*, 2003), but DRC4 was not (Supplemental Figure S3D). Thus DRC4 is not a major component of the protofilament ribbon, and any potential interaction between the ribbon and DRC4 is probably indirect.

Identification of DRC4-associated polypeptides by coimmunoprecipitation and iTRAQ analysis

To identify the polypeptides most closely associated with DRC4/PF2, we performed a series of coimmunoprecipitation experiments using extracts prepared from WT, mutant, and rescued axonemes. To define optimal conditions for immunoprecipitation, we incubated dialyzed extracts with CaM-IP2, GFP, and DRC4 antibodies and analyzed the resulting immunoprecipitates on Western blots probed with antibodies to CaM-IP3 and DRC4. As expected, the CaM-IP2 antibody immunoprecipitated CaM-IP3 but not DRC4, the DRC4 antibody immunoprecipitated DRC4 but not CaM-IP3, and the GFP antibody immunoprecipitated DRC4-GFP but not WT DRC4 (Supplemental Figure S3E). However, the WT DRC4 subunit (~55 kDa) migrated very close to the tubulin bands in the extract and the immunoglobulin bands in the immunoprecipitates, making it difficult to resolve DRC4 as a separate band. We therefore performed most immunoprecipitations using *PF2-HA* or *PF2-GFP* extracts, where DRC4 migrated at ~60 and ~75 kDa, respectively. Silver-stained gels revealed a large number of bands present in immunoprecipitates prepared from *PF2-HA* extracts relative to immunoprecipitates from control extracts (Figure 4A). Bands from both the HA-positive and control lanes were excised from the gel, extracted, trypsin digested, and analyzed by MS/MS. During the course of this study, we also identified FAP155 as the likely gene product of the *SUP-PF4* locus, based on the deletion of a large genomic region containing the *FAP155* gene (Lin *et al.*, 2011). We therefore transformed *sup-pf4* with a HA-tagged *FAP155* gene and performed additional immunoprecipitation experiments using WT, *sup-pf4*, and *SUP-PF4-HA* extracts (Supplemental Figure S4). Those polypeptides identified by minimum of three unique peptides in multiple experiments are listed in Table 1, and the individual peptides are shown in Supplemental Figure S5. Four polypeptides correspond to missing proteins identified by 2D gel-based methods (Lin *et al.*, 2011), but three polypeptides are novel: FAP122, FAP84, and FAP82 (Figure 4B). Western blots further demonstrated that the DRC1 subunit specifically coimmunoprecipitated with both DRC4-HA and FAP155-HA (Supplemental Figures 3E and 4D).

To confirm that the polypeptides identified by coimmunoprecipitation are bona fide subunits of the N-DRC, we analyzed WT and mutant axonemes by iTRAQ labeling and MS/MS. iTRAQ labeling

and mutant cells (right, *pf2-4* and *sup-pf3*) shows that the GFP signal is observed exclusively in the rescued strains. (C) The forward swimming velocities of WT, mutant, and rescued strains were measured by phase contrast microscopy. The total number of cells measured for each strain (n) is indicated. Both mutants were significantly slower than WT ($p < 0.005$). Rescued strains were faster than the mutant strains but not completely WT ($p < 0.005$). The *sup-pf3::PF2-GFP* rescued strains were also slightly but significantly slower than *pf2::PF2-GFP* ($p < 0.05$). (D) A Western blot of isolated axonemes was probed with antibodies against the DRC4 fusion protein antibody (top) and the RSP16 subunit (bottom). Truncated DRC4 subunits are found in *sup-pf3* and two rescued strains (left), whereas a larger, more abundant band at ~75 kDa is observed in the *PF2-GFP* rescued strains. (E) DIC and fluorescence images of dikaryons fixed at 10 and 30 min after mixing WT and *pf2-4::PF2-GFP* cells and stained with an antibody against GFP. No significant accumulation of the GFP signal was observed in the WT flagella. (F) Images of dikaryons fixed at 10 and 60 min after mixing *pf2-1* and *pf2-4::PF2-4-GFP* cells and stained with the GFP antibody. Accumulation of GFP signal was initially observed at the flagellar tips and gradually spread to the proximal region. Scale bars, 5 μm.

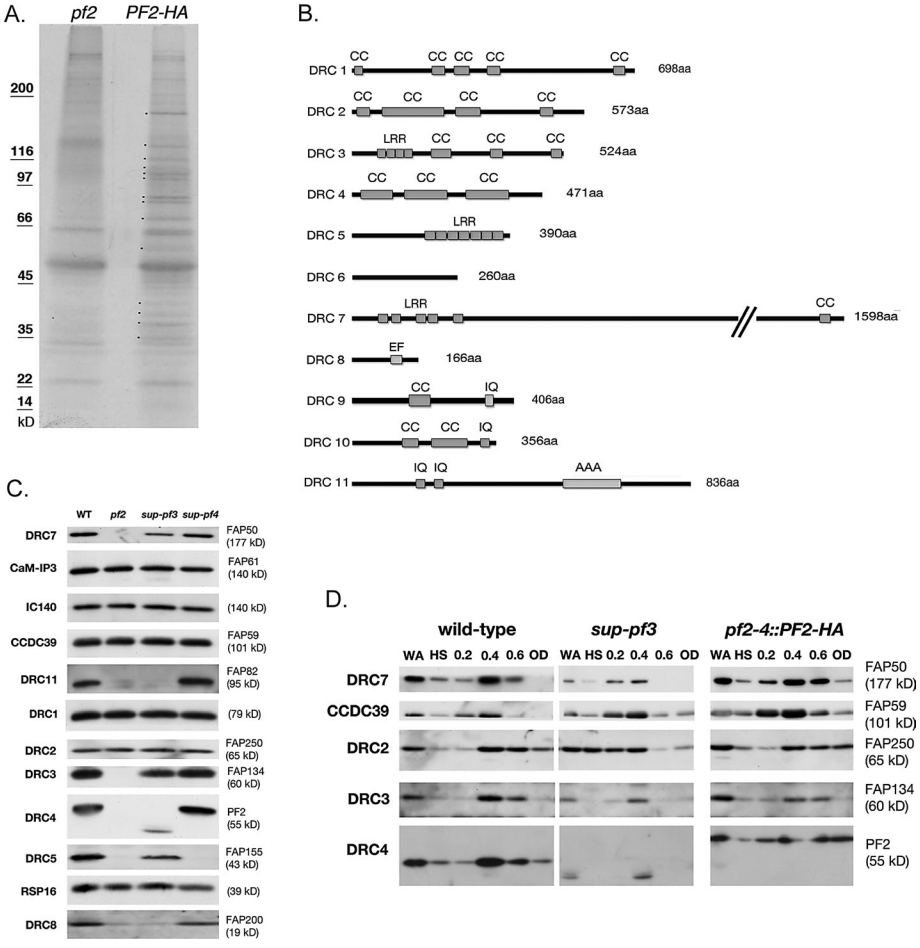

FIGURE 4: Identification of polypeptides that interact with DRC4. (A) Silver-stained gel of immunoprecipitates obtained with an HA antibody and extracts from *pf2* and *PF2-HA* axonemes. Although several polypeptides were nonspecifically bound to HA beads in both samples, several unique bands were observed in the *PF2-HA* sample. See Table 1 for polypeptides identified by MS/MS. (B) Diagrams showing predicted polypeptide domains in the candidate DRC subunits identified by coimmunoprecipitation and/or iTRAQ analyses. (C) Western blot of WT, *pf2*, *sup-pf3*, and *sup-pf4* axonemes probed with antibodies against candidate DRC subunits and other axonemal polypeptides. Several subunits identified as missing in *pf2* were also missing or reduced in *sup-pf3*. Only FAP155/DRC5 was missing in *sup-pf4*. Antibodies against subunits of the I1 dynein (IC140), CSC (FAP61/CaM-IP3), RS (RSP16), and FAP59/CCDC39 serve as loading controls. (D) Western blots of isolated axonemes (WA) and extracts obtained by sequential treatment with 0.6 M NaCl (HS), 0.2, 0.4, and 0.6 M NaI, and the final extracted outer doublets (OD). DRC subunits were coextracted from WT and *PF2-HA* with 0.4–0.6 M NaI, but some subunits were more readily extracted from *sup-pf3* at lower ionic strengths.

allows one to compare complex protein samples such as flagella and identify a small subset of polypeptides that are quantitatively different between samples (Portman *et al.*, 2009). Duplicate samples of WT and *pf2* axonemes were labeled with four different iTRAQ tags, digested with trypsin, fractionated by ion exchange and capillary LC, spotted on a matrix-assisted laser desorption/ionization (MALDI) target, and analyzed by mass spectrometry. A total of 252 polypeptides were identified with high confidence at a false discovery rate of 5%, and for most proteins, no significant differences were observed between WT and *pf2* samples. However, a small number of proteins were reproducibly reduced in *pf2*; these include all of the polypeptides identified by coimmunoprecipitation except FAP250 and DRC1 (Table 2). Other axonemal polypeptides, such as subunits of the RS, CSC, and protofilament ribbon, were unchanged. To verify these results, we raised antibodies against several candidates and used them to probe Western blots of WT, *pf2*, and *PF2-HA* axonemes. Antibodies against FAP50, FAP82, FAP134, FAP155, and FAP200 showed that each protein was present in WT, missing or reduced in *pf2*, and restored to WT levels in *PF2-HA* axonemes (Supplemental Figure S1B). Antibodies against other axonemal proteins, such the CaM-IP3 subunit of the CSC (FAP61), the IC140 subunit of the I1 dynein, and the RSP16 subunit of the RS, showed that the levels of these proteins were largely unchanged in *pf2* axonemes, consistent with the iTRAQ data. FAP250 was unchanged in *pf2* but reduced in *pf3* (Figure 1A), consistent with the hypothesis that FAP250 corresponds to DRC2 (Kabututu *et al.*, 2010; Lin *et al.*, 2011; Tritschler, Bower, and Porter, unpublished results).

Because *sup-pf3* and *sup-pf4* lack only a subset of the DRC subunits missing in *pf2*, we compared duplicate samples of WT, *pf2*, *sup-pf3*, and *sup-pf4* using iTRAQ labeling and an eight-plex analysis (Table 2). In this experiment, only 188 polypeptides were detected at a 5% false discovery rate, and the total number of peptides detected per protein was lower. The predicted protein ratios are likely less accurate (Mahoney *et al.*, 2011), but the general trends remained the same. Those proteins identified as reduced in *pf2* in the four-plex experiment were also reduced in the eight-plex experiment. The same proteins were reduced to a lesser extent in *sup-pf3*, and only two proteins (FAP169 and FAP155) were reduced in *sup-pf4*. Western blot analysis of WT, *pf2*, *sup-pf3*, and *sup-pf4* axonemes confirmed these observations (Figure 4C). The two proteins reduced in *sup-pf4* (FAP155 and FAP169) and two other proteins reduced in *pf2* and *sup-pf3* (FAP134 and FAP50) were recently identified by proteomic analysis of spots on 1D and 2D gels and designated as DRC5, DRC6, DRC3, and DRC7, respectively (Lin *et al.*, 2011). However, FAP200, FAP122, FAP84, and FAP82 are candidates for additional DRC subunits, now designated as DRC8–DRC11 (see Table 2, Figure 4B, and Supplemental Figure S5). Furthermore, these proteins contain domains (EF hand, IQ domains) implicated in calcium signaling, and DRC11 also contains an AAA domain typically associated with nucleotide hydrolysis (Figure 4B).

Coextraction and cosedimentation of DRC subunits

Because *drc* mutations disrupt the assembly of several distinct axonemal structures (Gardner *et al.*, 1994; Heuser *et al.*, 2009), it is critical to determine whether the polypeptides associated with DRC4 are bona fide subunits of the same protein complex or components of peripheral structures. We therefore analyzed high-salt extracts by sucrose density gradient centrifugation and Western blots. As mentioned earlier, DRC4 was extracted from WT axonemes

Protein	Molecular weight (kDa)	DRC4-HA (peptides, spectra)	DRC5-HA (peptides, spectra)
DRC1	79	WB	WB
FAP250 (DRC2)	65	7 (21)	6 (6)
FAP134 (DRC3)	60	3 (3)	4 (4)
PF2 (DRC4)	55	4 (6)	9 (10)
FAP155 (DRC5)	43	WB	3 (6)
FAP50 (DRC7)	177	21 (64)	15 (20)
FAP122 (DRC9)	46	6 (11)	8 (14)
FAP84 (DRC10)	41	7 (20)	7 (10)
FAP82 (DRC11)	95	WB	5 (6)

Both the total number of unique peptides and the total number of assigned spectra are shown. WB indicates a protein that was not identified in the initial mass spectroscopic analysis but was subsequently detected in the immunoprecipitates by Western blots (Supplemental Figures S3 and S4).

TABLE 1: Polypeptides identified by coimmunoprecipitation with DRC4 and DRC5.

in ~0.5 M NaI, along with subunits of the RS and CSC (Supplemental Figure S3A). Reprobing the blots with antibodies against several N-DRC candidates confirmed that these proteins were also preferentially extracted in 0.5 M NaI (Supplemental Figure S3A). To determine whether the N-DRC could be physically separated from the RS and CSC, we dialyzed the high-salt extracts against low salt and fractionated by sucrose density gradient centrifugation. DRC4 sedimented at >19 S in WT extracts, in a region that overlaps with subunits of the RS and CSC complexes (Supplemental Figure S3F). However, sedimentation of DRC4 was unchanged in *pf14* extracts that lack the RS, even though the CSC was shifted to the upper portion of the gradient (Supplemental Figure S3G). These observations demonstrate that DRC4 is part of a discrete complex distinct from both the RS and the CSC. Sedimentation of the RS and CSC was unchanged in *pf2* extracts (Supplemental Figure S3H), consistent with this hypothesis. We therefore analyzed extracts from WT, mutant, and rescued strains to assess which DRC subunits might be most closely associated with DRC4.

Because loss of one DRC subunit might affect extraction of other DRC components, we extracted axonemes sequentially with

Complex name	Protein	Four-plex peptides	WT/WT	*pf2*/WT	Eight-plex peptides	WT/WT	*pf2*/WT	*sup-pf3*/WT	*sup-pf4*/WT
DRC1		14(17)	0.88	0.84	8 (10)	0.67	1.37	1.04	1.40
DRC2	FAP250	6(9)	0.96	0.92	5 (10)	1.12	1.00	0.99	1.03
DRC3	FAP134	4(5)	0.96	**0.07**	2 (2)	1.05	**0.55**	**0.72**	1.08
DRC4	PF2	15(16)	1.11	**0.07**	4 (4)	1.00	**0.36**	**0.62**	1.00
DRC5	FAP155	1(2)	0.89	**0.11**	1 (1)	0.86	**0.40**	**0.47**	**0.37**
DRC6	FAP169	4(4)	1.02	**0.11**	1 (1)	1.09	**0.24**	**0.35**	**0.20**
DRC7	FAP50	10(12)	0.94	**0.06**	4 (4)	1.00	**0.61**	**0.68**	1.01
DRC8	FAP200	2(5)	1.07	**0.12**	1 (1)	1.02	**0.44**	**0.30**	0.95
DRC9	FAP122	3(3)	1.02	**0.06**	3 (2)	1.08	**0.50**	**0.66**	1.18
DRC10	FAP84	2(2)	1.05	**0.34**	ND				
DRC11	FAP82	2(2)	0.91	**0.43**	1 (1)	0.90	**0.50**	**0.41**	1.28
Ribbon	Rib43a	19(25)	0.99	0.98	12 (16)	1.12	0.76	0.82	1.23
Ribbon	Rib72	53(62)	0.97	1.08	28 (38)	1.37	1.58	1.41	1.50
CCDC39[a]	FAP59	17(19)	0.98	1.01	5 (11)	1.07	0.98	0.98	0.99
CaM-IP3	FAP61	7(9)	0.94	0.89	2 (3)	1.08	0.97	0.90	0.93
CaM-IP4	FAP251	6(6)	0.96	0.98	4 (6)	0.97	1.05	1.05	1.04
Radial spoke	RSP16	20(30)	1.03	1.19	14 (12)	0.98	0.96	0.94	0.97
MBO	MBO2	5(6)	0.91	0.92	1(2)	1.01	0.90	0.99	0.96

The relative amount of each protein in each sample was compared with that present in the WT sample to obtain a protein ratio. The WT/WT ratios indicate the variability in labeling and protein loading between replicates of the same sample (typically <10%). For each protein, duplicate mutant/WT ratios were averaged. Proteins whose mutant/WT ratios were <75% in both experiments are indicated in bold, with the exception of FAP84, which was only detected in the four-plex experiment. The total number of unique peptides detected at the 95% confidence interval is shown first, and the number of peptides used for quantification is indicated in parentheses.

[a]CCDC39 is the name of the human orthologue of FAP59.

TABLE 2: Polypeptide ratios in WT and *drc*-mutant axonemes determined by iTRAQ analysis.

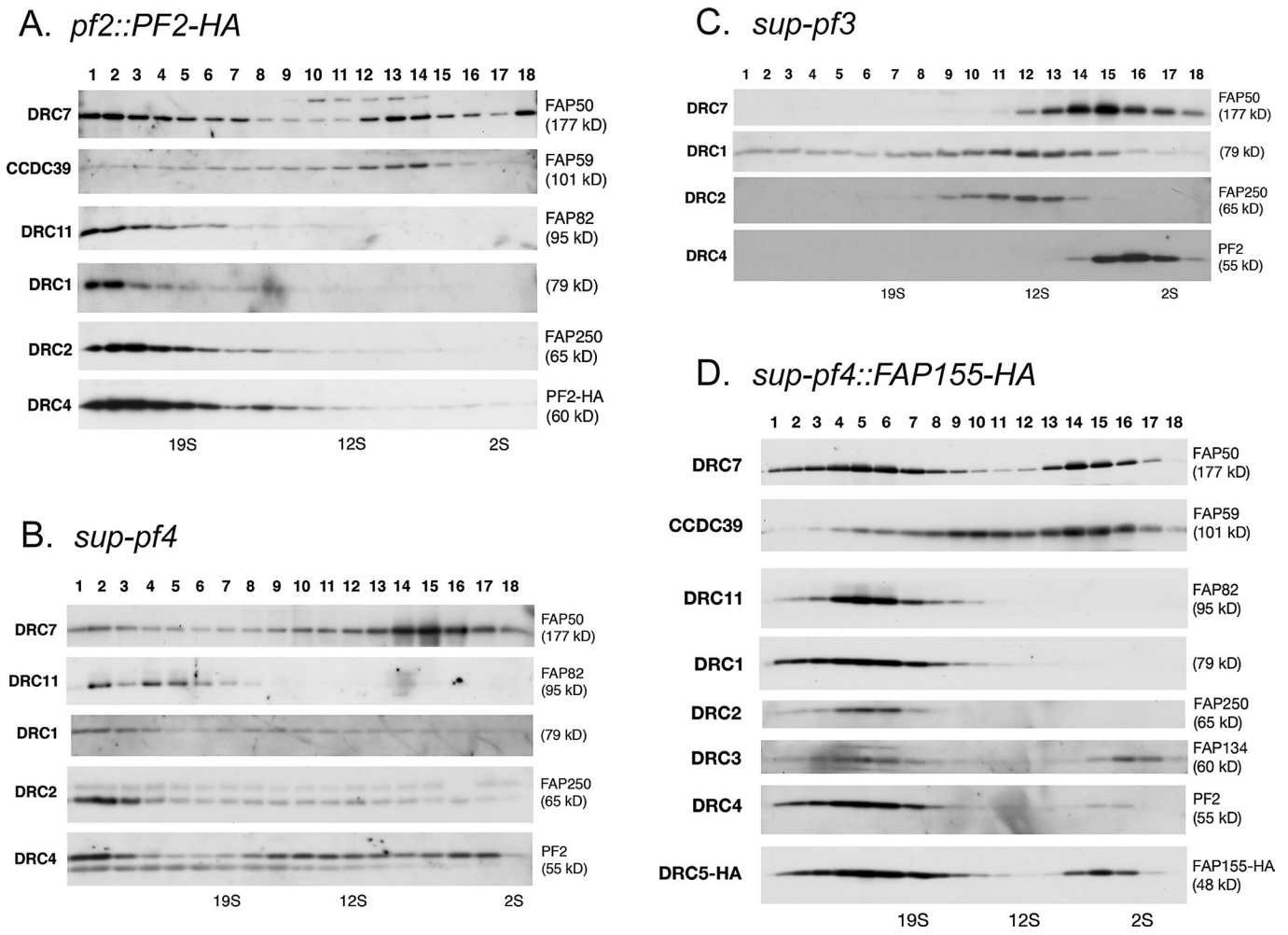

FIGURE 5: Sucrose density gradient centrifugation identifies subcomplexes within the DRC. Western blots of fractions obtained by analyzing DRC-containing extracts on 5–20% sucrose density gradients. The bottoms (20% sucrose) of the gradients are on the left. (A) *PF2-HA,* all DRC subunits cosediment near the bottom of the gradient; (B) *sup-pf4,* DRC subunits dissociate into multiple peaks; (C) *sup-pf3,* DRC subunits form three distinct subcomplexes; (D) *SUP-PF4-HA,* most DRC subunits reassociate to form a large complex that sediments near the bottom of the gradient.

different salt solutions to identify optimal conditions for release of the DRC. For instance, *sup-pf3* axonemes lack a subset of DRC polypeptides (Table 2 and Figure 4C), and the *sup-pf3* mutation deletes a conserved region of DRC4 (Figure 1B) that overlaps with a predicted microtubule-binding site (Bekker *et al.*, 2007). The modified DRC4 subunits might therefore be more readily extracted from *sup-pf3* axonemes in buffers of lower ionic strength. However, the DRC4 subunits in *sup-pf3* were not released until treatment with 0.4 M NaI (Figure 4D), which suggests that the interaction of DRC4 with the outer doublet was not significantly altered in *sup-pf3*. In contrast, some of the other DRC subunits were more easily extracted from *sup-pf3* axonemes than from WT or *PF2-HA* axonemes (Figure 4D). This susceptibility to salt extraction was most obvious with DRC2. A significant proportion of DRC2 was released at each step in the 0.6 M NaCl, 0.2 M NaI, and 0.4 M NaI extracts, and very little protein remained in the 0.6 M NaI extract or final pellet of outer doublets. In contrast, DRC2 was not released from WT or *PF2-HA* axonemes until treatment with 0.4–0.6 M NaI, and even then, a significant fraction remained bound to the final pellet of outer doublets. Similar effects were observed with other DRC subunits (Figure 4D). These results suggest that even though DRC2 is present at WT levels in *sup-pf3*, the defects in DRC4 weaken its interactions with other DRC subunits, including DRC2.

To further explore the relationship between the different DRC subunits, we subjected extracts from several strains to sucrose density gradient centrifugation and analyzed the resulting fractions on Western blots. DRC subunits present in extracts prepared from WT and HA rescued strains were observed to cosediment near the bottom (>19 S) of 5–20% sucrose density gradients, although a significant portion of DRC7 was also observed near the top of the gradient at ~8 S (Figure 5 and Supplemental Figure S3F). In contrast, several other proteins sediment near the top of the gradients, including Rib43, Rib72, and tektin (Supplemental Figure S3F). FAP59 is the *Chlamydomonas* orthologue of the CCDC39 protein in humans, which was recently proposed as a potential DRC subunit (Merveille *et al.*, 2011). However, FAP59 did not appear to be very tightly associated with the DRC in *Chlamydomonas*, as it also sedimented near the top of the sucrose gradients (Figure 5 and Supplemental Figure S3F). Thus only a subset of the proposed DRC subunits cosediment as a discrete complex on gradients of WT and rescued extracts.

The *sup-pf4* mutant is the least defective *drc* mutant identified to date (Huang *et al.*, 1982). Its motility phenotype is difficult to

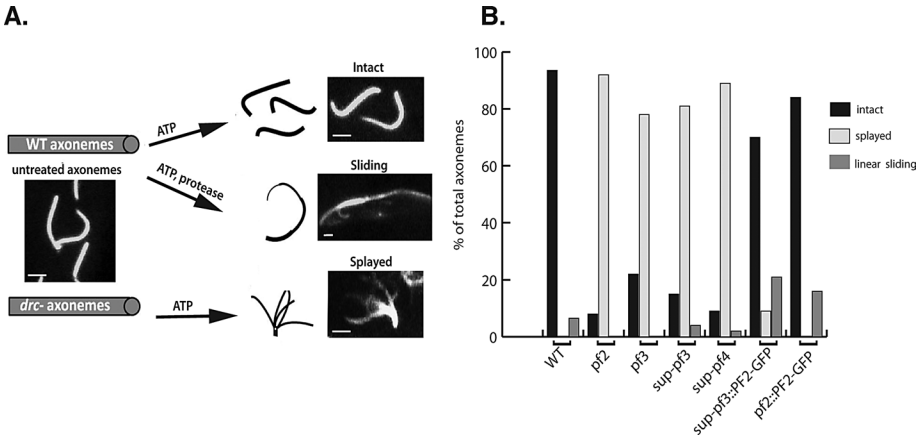

FIGURE 6: The N-DRC maintains alignment between outer doublet microtubules in the presence of ATP. (A) Responses of full-length WT or mutant axonemes upon addition of 0.1 mM ATP or 0.1 mM ATP and protease. (B) Quantification of the numbers of axonemes that remained intact, splayed at their distal ends, or underwent sliding disintegration in the presence of 0.1 mM ATP alone. The majority of WT axonemes remained intact (and occasionally were observed to reactivate flagellar beating), whereas axonemes from *drc*-mutant strains splayed at their distal ends. Axonemes from rescued strains remained intact. Scale bar is 4 μm.

distinguish from WT (Brokaw and Luck, 1985; Gardner *et al.*, 1994), and only a small portion of the linker domain is missing when analyzed by cryo-ET (Heuser *et al.*, 2009). Only two polypeptides (DRC5 and DRC6) are missing in *sup-pf4* axonemes (Table 2; Huang *et al.*, 1982; Piperno *et al.*, 1992, 1994; Lin *et al.*, 2011). However, analysis of *sup-pf4* extracts suggests that loss of DRC5 and DRC6 destabilizes other subunits of the N-DRC. For example, DRC7 was more readily solubilized than DRC2 and DRC4 in *sup-pf4* extracts (Supplemental Figure S4C). Second, DRC4 and DRC7 dissociated into multiple peaks on *sup-pf4* gradients, but DRC1, DRC2, and DRC11 still cosedimented near the bottom (Figure 5B). However, after rescue of *sup-pf4* with the *FAP155-HA* construct, all of the DRC subunits reassociated and cosedimented on the *SUP-PF4-HA* gradient (Figure 5D).

The dissociation of the N-DRC was even more pronounced in *sup-pf3* gradients (Figure 5C). Truncated DRC4 subunits were always observed near the top of the gradient, peaking in fraction 16. DRC7 sedimented slightly further down, peaking in fraction 17, and DRC1 and DRC2 cosedimented near the middle of the gradient as a third peak in fractions 11–13. The dissociation of the N-DRC into at least three distinct subcomplexes in *sup-pf3* is consistent with its greater susceptibility to salt extraction described earlier (Figure 4D) and further highlights the central role of DRC4 in the assembly of the N-DRC linker.

Evidence for the role of the N-DRC subunits in maintaining outer doublet alignment and limiting microtubule sliding

Based on diverse data, the nexin link of the N-DRC is postulated to play a role in the alignment of adjacent doublet microtubules and the maintenance of the integrity of the axoneme (Gibbons, 1963, 1965; Stephens, 1970; Stephens *et al.*, 1989; Summers and Gibbons, 1971, 1973; Linck, 1973; Witman *et al.*, 1978; Heuser *et al.*, 2009; Porter, 2012). To address this hypothesis, we isolated full-length axonemes from WT, *drc* mutants, and rescued strains and tested their ability to undergo either ATP-induced reactivation or microtubule-sliding disintegration (Figure 6). When full-length, WT axonemes were incubated with 0.1 mM ATP in the absence of protease, they often exhibited cycles of reactivated beating, but the axonemes remained intact. Once protease was added to WT axonemes, 0.1 mM ATP induced linear microtubule-sliding disintegration of the axonemes (Figure 6A), as previously described (Okagaki and Kamiya, 1986; Smith and Sale, 1992). In contrast, when full-length axonemes from *drc* mutants were incubated in the presence of 0.1 mM ATP, they were observed to fray into individual doublets at their distal ends but remained intact at their proximal ends (Figure 6). Of interest, pairs or small subsets of doublets often displayed cycles of repetitive microtubule sliding and bending, similar to that observed previously with protease-treated WT axonemes (Aoyama and Kamiya, 2005). However, the splayed *drc*-mutant axonemes rarely exhibited complete sliding disintegration in the absence of protease (Figure 6). Addition of both ATP and protease to *drc*-mutant axonemes induced splaying, followed by microtubule sliding and disintegration. Isolated axonemes from the rescued strains remained intact and did not splay in the presence of ATP alone (Figure 6B), demonstrating that the structural connections between the outer doublets were restored in the rescued strains. In addition, axonemes from the rescued strains displayed linear microtubule sliding disintegration when treated with both ATP and protease, similar to WT axonemes (Figure 6A).

Thus, as predicted, addition of ATP alone to *drc*-mutant axonemes resulted in the active disruption of the axoneme by splaying of doublet microtubules. However, the experiments also revealed that the outer doublets are held together at the proximal end of the axoneme. These results suggest that additional structures, presumably sensitive to added proteases, must be present in the proximal region of the axoneme and that these proximal structures help to maintain the 9 + 2 arrangement of the axoneme in the absence of N-DRC connections (see *Discussion*).

DISCUSSION

DRC4 plays a central role in the assembly of the N-DRC linker

DRC4 is one of the most highly conserved subunits of the N-DRC, and closely related sequences have been identified in nearly all species with motile axonemes (Table 3; Rupp and Porter, 2003; Ralston and Hill, 2006; Merchant *et al.*, 2007; Colantonio *et al.*, 2009; Hodges *et al.*, 2011). Characterization of *sup-pf3* as a transposon-induced, in-frame deletion in the *PF2* gene (Figure 1 and Supplemental Figure S2) further demonstrates that DRC4 plays a central role in the assembly and function of the N-DRC linker. The identification of *sup-pf3* as a *PF2* allele was unexpected, given that *sup-pf3* was previously mapped to linkage group VI (Huang *et al.*, 1982), but rescue by transformation with *PF2* (Figure 2) clearly shows that *sup-pf3* and *pf2* are two mutations in the same gene on linkage group IX. These observations are also consistent with the similarities in their biochemical and structural phenotypes (Piperno *et al.*, 1992, 1994; Gardner *et al.*, 1994; Heuser *et al.*, 2009). The presence of a large *TOC1* transposon within the *PF2* gene might have been expected to completely block its function, but alternative splicing to remove *TOC1* has been observed in other genes (Rushforth and Anderson, 1996). Moreover, the modified DRC4 subunits in *sup-pf3* clearly retain some function. Although the amount of DRC4 is reduced (Figures 1A, 2D, and 4C and Table 2), binding of DRC4 to the outer doublet does not appear to be significantly altered, as

DRC (molecular weight, kDa)	FAP (amino acids)	*Chlamydomonas* V5.3 (chromosome: base pairs)	*Homo sapiens*	*Micromonas pusilla*	*Physcomitrella patens*	*Thalassiosera pseudonana*
DRC1 (79)	(698)	Linkage group VIII AFU81554	CCDC134, BAB71385.1 4e-107 (13–698)	XP_002506453.1 2e-125 (51–694)	XP_001763650.1 2e-97 (32–685)	XP_002295435.1 4e-27 (50–388, 640–698)
DRC2 (65)	FAP250 (573)	13: 5161606–5166247	CCDC65, NP_149115.2 5e-81 (33–518)	XP_003064697.1 4e-98 (56–388, 465–522)	XP_001772998.1 1e-66 (19–499)	XP_002292217.1 8e-34 (61–523)
DRC3 (60)	FAP134 (524)	12: 5555729–5560239	LRRC48, NP_001123562.1 8e-84 (11–515)	XP_003055857.1 9e-100 (12–508)	XP_001780284.1 1e-60 (11–508)	ND
DRC4 (55)	PF2 (471)	11: 2697085–2703306 AAP57169.1	GAS11, NP_001472.1 5e-141 (1–468)	EEH59759.1 8e-153 (7–471)	XP_001752545.1 1e-132 (24–460)	XP_002288239.1 8e-32 (58–434)
DRC5 (43)	FAP155 (390)	1: 6359148–6363883	TCTE1, NP_872345 1e-63 (7–380)	XP_002505379.1 6e-80 (7–367)	ND	ND
DRC6 (28)	FAP169 (260)	12: 3772048–3774891	CAD28506.1 0.084 (63–219)	XP_003056139.1 1e-27 (64–198)	XP_001781452.1 4e-20 (23–225)	ND
DRC7 (177)	FAP50 (1598)	14: 733010–747385	CCDC135, EAW82949.1 1e-62 (614–1598)	XP_003057247.1 2e-177 (11–1593)	XP_001766850.1 8e-140 (20–1590)	ND
DRC8 (19)	FAP200 (166)	16: 6910046–6912757	EFCBD2, NP115704.1 2e-16 (1–162)	ND	ND	XP_002295755.1 1e-14 (13–159)
DRC9 (46)	FAP122 (406)	1: 3911197–3914171	IQCG, AAH04816.2 1e-05 (133–391)	XP_003055608.1 2e-31 (57–349)	ND	ND
DRC10 (41)	FAP84 (356)	2: 7902751–7906536	IQCD, Q96DY2.2 4e-12 (1-333)	ND	ND	ND
DRC11 (95)	FAP82 (836)	7: 2048046–2058557	IQCA1, NP_079002.3 7e-146 (1–836)	XP_002504754.1 8e-179 (1–831)	XP_001767278.1 8e-114 (5–800)	XP_002294237.1 3e-48 (1–727)

The total number of amino acids and predicted molecular weights are based on data in the most recent release of the *Chlamydomonas* genome (V5.3). The DRC1 cDNA sequence was not detected in the genome project but has been recently released and mapped to linkage group VIII (Wirschell *et al.*, 2013). The polypeptide sequences were used to BLAST search the National Center for Biotechnology Information database and identify the most closely related sequences in humans, *Micromonas* (a widely distributed, phototactic green alga with a small genome; Worden *et al.*, 2009), *Physcomitrella* (a bryophyte moss with flagellated sperm and inner dynein arms but no outer dynein arms; Rensing *et al.*, 2008), and *Thalassiosera* (a centric diatom with flagellated sperm and outer dynein arms but no inner dynein arms, central pair microtubules, or radial spokes; Armbrust *et al.*, 2004). The name (if available) and accession number of the best hits are shown, along with the BLAST score and the region of alignment (in parentheses). ND, no closely related sequence was detected.

TABLE 3: DRC subunits identified in *Chlamydomonas* and orthologues in other species.

assayed by its resistance to extraction (Figure 4D and Supplemental Figure S3), even though the deleted region overlaps with a proposed microtubule-binding domain (Bekker *et al.*, 2007). In addition, *sup-pf3* axonemes contain higher levels of DRC3, DRC5, and DRC7 than *pf2* (Figure 4C and Table 2). Thus the truncated DRC4 subunits in *sup-pf3* must retain some binding sites for interaction with other DRC subunits.

The residual N-DRC also appears to be stably associated in vivo, as evidenced by the failure to complement *sup-pf3* by mating to WT cells in temporary dikaryons (Huang *et al.*, 1982). These results imply that DRC4 bound to outer doublets does not readily exchange with cytoplasmic precursors. To test this hypothesis directly, we mated *PF2-GFP* cells to both *pf2* and WT cells and examined temporary dikaryons for the appearance of DRC4-GFP in unlabeled flagella (Figure 2, E and F). DRC4-GFP signal was detected at the tips of *pf2* flagella soon after mating but was not seen in WT flagella after 1 h. These observations indicate that DRC4 is part of a complex that must be transported to and/or modified at the flagellar tip for proper assembly and that turnover of DRC4 is relatively slow in the presence of endogenously bound complex. Additional work is needed to identify the components involved in the transport and modification of the N-DRC during flagellar assembly. Recent studies show that the assembly of RS in vivo is a complex, multistep process that requires IFT, LC8 binding to the RS stalk at the flagellar tip, and phosphorylation of RS subunits before attachment to the outer doublet (Gupta *et al.*, 2012).

The N-DRC stabilizes the attachment of dynein *e* (DHC8) to the axoneme

Several studies proposed that the N-DRC functions as an adaptor for the binding of a subset of inner-arm dyneins to the outer doublets (Piperno *et al.*, 1992, 1994; Gardner *et al.*, 1994). However, the complexity of DHC composition and the heterogeneity in DHC distribution both around and along the length of the axoneme have complicated efforts to identify the specific dyneins affected (Bui *et al.*, 2009; Yagi *et al.*, 2009). Quantification of inner-arm DHCs by spectral counting demonstrated that DHC8 is significantly reduced in *pf2* and restored to WT levels in *PF2-HA* axonemes (Figure 3), consistent with previous speculation that the IA4 structure corresponds to dynein *e* (Gardner *et al.*, 1994; Bui *et al.*, 2009; Heuser *et al.*, 2009). No significant changes were observed in DHC5 (dynein *b*), unlike our previous study based on the FPLC analysis of dynein extracts (Gardner *et al.*, 1994), but a slight decrease was detected with DHC2 (dynein *d*). Additional work is needed to identify the other DHCs most closely associated with the DRC. Recent studies suggest that both DHC2 (dynein *d*) and DHC7 (dynein *g*) may be located in this region (Bui *et al.*, 2012) and also confirm that DHC8 is reduced in *pf2* (Kubo *et al.*, 2012). The inner-arm DHC defects detected by spectral counting in *pf2* are also consistent with the recent characterization of DHC defects in *pf3* (Wirschell *et al.*, 2013) and the earlier description of these strains as inner-arm motility mutants (Brokaw and Kamiya, 1987).

The N-DRC is a discrete, tightly bound axonemal complex

Although the N-DRC is believed to mediate signals between the radial spokes and dynein arms (Piperno *et al.*, 1992, 1994; Gardner *et al.*, 1994; Heuser *et al.*, 2009), the nature of the biochemical interactions between these different structures is poorly understood. We therefore generated epitope-tagged DRC constructs and several antibodies against DRC subunits as tools for the analysis of the N-DRC in vivo and in vitro (Supplemental Tables S1 and S4 and Supplemental Figure S1). Biochemical fractionation revealed that DRC4 is highly enriched in isolated flagella and axonemes relative to the cell body or flagellar membrane fraction (Figure 2 and Supplemental Figure S3A). Moreover, DRC4 is uniformly distributed along the length of the axoneme when viewed by fluorescence microscopy (Figure 2), consistent with previous work (Rupp and Porter, 2003). DRC4 and other DRC subunits are most efficiently extracted with 0.4–0.6 M NaI, along with subunits of the RS and CSC (Figure 4 and Supplemental Figure S3A). However, DRC subunits can be separated from subunits of the RS, CSC, or protofilament ribbon by differential extraction and/or by sucrose density gradient centrifugation of WT or mutant extracts (Figure 4 and Supplemental Figure S3), consistent with the hypothesis that the N-DRC is a discrete complex.

Coimmunoprecipitation and iTRAQ analysis have identified 10 polypeptides closely associated with DRC4 (Tables 1 and 2), including four subunits not previously identified by 2D gel-based approaches (Lin *et al.*, 2011). To verify these observations, we generated antibodies to six of the DRC candidates (Supplemental Figure S1). All except FAP250 are missing or reduced in *pf2* (Figure 4). However, FAP250 is missing or reduced in *pf3* (Figure 1). The *pf3* mutant is associated with defects in assembly of the DRC1 and DRC2 subunits (Huang *et al.*, 1982; Piperno *et al.*, 1992, 1994; Lin *et al.*, 2011) believed to be major components of the N-DRC base plate (Heuser *et al.*, 2009). We propose that FAP250 corresponds to DRC2 based on the similarities in their predicted molecular weights (65 and 73 kDa. respectively). In addition, the gene encoding FAP250 maps to chromosome 13, whereas the gene encoding DRC1 has been linked to *pf3* mutation on chromosome 8 (Piperno *et al.*, 1994; Wirschell *et al.*, 2013). Therefore we have strong evidence for at least 11 DRC subunits.

At least six DRC subunits cosediment with DRC4 as part of a large complex in extracts from WT and rescued strains, but the N-DRC dissociates into smaller subcomplexes in *drc*-mutant extracts (Figure 5 and Supplemental Figure S3). In particular, the loss of DRC5 and DRC6 destabilizes the interaction between DRC7 and DRC4 in *sup-pf4* extracts (Figure 5B and Supplemental Figure S4C), and the truncation of DRC4 in *sup-pf3* leads to the loss of DRC11 and the formation of at least three distinct subcomplexes (Figure 5C). Antibodies to other DRC subunits are needed to further characterize the individual subcomplexes.

Significant defects in the assembly of ICL1, IC140, or FAP61 were not observed in *pf2*, *sup-pf3*, or *sup-pf4* axonemes by either iTRAQ or Western blot analyses (Figure 4). These results differ from previous observations based on 2D gels (Lin *et al.*, 2011). The reasons for this discrepancy are unknown but may reflect the difficulties associated with the resolution of higher–molecular weight polypeptides on 2D gels. We previously found evidence for changes in the phosphorylation status of FAP119, FAP206, FAP230, and FAP252 in several *n-drc* mutants (Lin *et al.*, 2011). Of interest, FAP206 was recently recovered by coimmunoprecipitation with RSP3 (Gupta *et al.*, 2012), and FAP252 was previously associated with Rib72 based on blot overlay (Ikeda *et al.*, 2007). These polypeptides may therefore be associated with structures that are located in close proximity to the N-DRC, but whether they represent bona fide N-DRC subunits is unresolved. Our current understanding of N-DRC subunit composition is summarized in Supplemental Table S4.

Characteristics and distribution of DRC subunits

Most DRC subunits are structural proteins that are widely conserved in species that assemble motile axonemes (Table 3; Merchant *et al.*, 2007; Hodges *et al.*, 2011; Lin *et al.*, 2011). Eight subunits contain coiled-coil domains and/or leucine-rich repeats likely to be important for subunit interactions and complex assembly (Figure 3B). However, four new DRC candidates (DRC8–DRC11) contain EF hand or IQ domains involved in binding calcium- or calmodulin-related proteins. Whether any of these subunits also interacts with RS2 and/or the CSC remains to be determined. DRC11 also contains an AAA domain typically associated with nucleotide binding and hydrolysis (Snider and Houry, 2008). Whether the IQ domain or the AAA domain of DRC11 contributes to the proposed conformational changes of the nexin link (Bozkurt and Woolley, 1993; Minoura *et al.*, 1999; Lindemann *et al.*, 2005; Lindemann, 2011) is unknown but is an intriguing possibility. Furthermore, the absence of DRC11 in both *pf2* and *sup-pf3* suggests that it may correspond to one of the two unidentified densities in the linker region of the N-DRC that makes contact with the neighboring B-tubule (Heuser *et al.*, 2009).

The identification of additional mutant alleles will be an important next step toward understanding the contribution of each subunit in assembly and/or motility. For instance, the characterization of the *pf3* mutation in DRC1 and another mutation in the human orthologue CCDC135 demonstrates that this DRC subunit plays a conserved role in assembly of the N-DRC and ciliary motility (Wirschell *et al.*, 2013). A FAP134 (DRC3) mutant has been identified (Lechtreck *et al.*, 2009a), but little is known about its motility phenotype or effects on the assembly of other DRC subunits. DRC3 has been associated with DRC4 based on its presence in *sup-pf3* and absence in *pf2* (Huang *et al.*, 1982; Piperno *et al.*, 1992, 1994; Lin *et al.*, 2011). DRC3 might be one of the 65- to 85-kDa polypeptides that interact directly with DRC4 using chemical cross-linking (Rupp and Porter, 2003).

A mutation has been identified in the *Drosophila* orthologue of DRC7 known as CG34110/CCDC135 (Yang *et al.*, 2011). The *lost boys* (*lobo*) mutation was recovered by screening for defects in the movement of *Drosophila* sperm in the female reproductive tract, a calcium-regulated process that requires both waveform conversion and regulation of wave propagation. The *lobo* phenotype is similar to that of a *Pkd2* mutant that disrupts a polycystin-related calcium channel in the flagellar membrane, and so the authors proposed that CG34110 functions downstream of Pkd2 in a common signaling pathway (Yang *et al.*, 2011). Because no calcium-binding domain has been identified in CG34110, some other DRC subunits with calcium- or calmodulin-binding domains may also be involved in this pathway. Phylogenetic comparisons of ciliary proteins have recently identified a conserved transglutaminase-like (TGL) peptidase domain in CCDC135/CG34110/FAP50 that is predicted to bind tightly to glutamylated proteins (Zhang and Aravind, 2012). If the TGL domain is functional in DRC7, it might facilitate interactions with glutamylated tubulin residues on the B-tubule. Of interest, a recent study of a glutamylation-deficient strain (*tpg1*) provided evidence for an interaction between glutamylated tubulin and dynein *e* and the DRC during microtubule sliding (Kubo *et al.*, 2010, 2012).

The total mass of DRC subunits identified thus far is ~750 kDa, about half the size of the N-DRC estimated by cryo-ET (Heuser *et al.*, 2009). Nothing is known about the absolute stoichiometry of the subunits, but it is possible to use the flagellar proteome (Pazour *et al.*, 2005) to estimate the relative stoichiometries of the DRC subunits compared with other flagellar proteins, as done previously for subunits of the IFT and BBS complexes (Lechtreck *et al.*, 2009b). These estimates assume that the total number of peptides detected per polypeptide is roughly proportional to the size of the protein and its relative abundance in the flagellum. Several peptides were detected for each DRC subunit, ranging from 1.7 to 3.3 peptides per 10 kDa, with an average of ~2.5 peptides per 10 kDa. These ratios are similar to those obtained for subunits of the CSC (1.1–2.1 peptides/10 kDa) and FAP59 (2.5 peptides/10 kDa) but approximately one-half of those observed for RSP3 (4.8 peptides per 10 kDa). Current models of the RS vary considerably in their estimates of RSP subunit stoichiometries (Yang and Smith, 2009; Pigino *et al.*, 2011), but the only direct evidence indicates that RSP3 is present as a dimer (Wirschell *et al.*, 2008). In addition, the DRC and CSC are associated with only one spoke (RS2) per 96-nm repeat (Gardner *et al.*, 1994; Heuser *et al.*, 2009, 2012a). Based on these estimates, each N-DRC structure could contain two copies of each subunit, which would total ~1500 kDa, close to the size of the N-DRC estimated by cryo-ET (Heuser *et al.*, 2009). Further work is needed to purify the N-DRC and determine the stoichiometry of each subunit directly.

Orthologues of the DRC subunits are widely distributed in organisms with motile axonemes (Merchant *et al.*, 2007; Hodges *et al.*, 2011), including species such as *Physcomitrella* that lack outer dynein arms but retain radial spokes and inner dynein arms (Rensing *et al.*, 2008; Table 3). Of interest, however, at least four of the DRC subunits (DRC1, DRC2, DRC4, and DRC11) are also retained in species such as *Thalassiosira* that only assemble outer dynein arms but lack the CP/RS complex and inner dynein arms (Armbrust *et al.*, 2004). These comparisons suggest that the N-DRC plays a fundamental role in regulating motility that is even more basic than the higher-order control provided by the CP/RS complex. Indeed others have noted that both microtubule spacing and interdoublet linkages are highly conserved in motile 9 + 0 cilia (Lindemann, 2011). In addition, DRC subunits have not been detected in nonmotile primary cilia (Ishikawa *et al.*, 2012). The latter is consistent with the observations that the organization of the outer doublets is often more variable in primary cilia than in motile cilia (Gluenz *et al.*, 2010). Taken together, these observations suggest the primary function of the N-DRC is to maintain outer doublet alignment in motile axonemes and limit microtubule sliding during flagellar bending. To further test this idea, we examined ATP-induced reactivation and dynein-driven microtubule sliding in *drc*-mutant axonemes.

The N-DRC maintains the alignment and integrity of the distal axoneme

The discovery that the DRC is a component of the nexin link that interconnects outer doublet microtubules (Heuser *et al.*, 2009) was somewhat unexpected, given that two of the *drc* mutants display near-wild-type motility (Brokaw *et al.*, 1982; Brokaw and Luck, 1985). In addition, no significant defects in axoneme organization had been observed, with the caveat that the samples had been prepared in the absence of ATP (Gardner *et al.*, 1994; Heuser *et al.*, 2009). Based on the hypothesis that the N-DRC contains at least some of the protease-sensitive components that normally maintain the integrity of the isolated axoneme (Summers and Gibbons, 1971, 1973), we predicted that addition of ATP to axonemes with N-DRC deficiencies would result in dynein-driven microtubule sliding and axoneme disintegration rather than ATP-induced reactivation of axonemal bending. However, in full-length, unsonicated axonemes, the disruption occurred by the splaying of individual outer doublet microtubules in the medial and distal regions of the axoneme. In contrast, the proximal ~2 μm of the *drc*-mutant axonemes remained intact (Figure 6).

These results are consistent with a model in which the N-DRC plays a role in maintaining the alignment of outer doublets in the medial/distal region of the axoneme during motility. In the absence of N-DRC connections, the integrity of the isolated axoneme and alignment of outer doublets are apparently maintained by the dynein arms: addition of ATP to the *drc* mutant axonemes leads to dynein arm detachment and results in splaying of the outer doublet microtubules. In addition, we frequently observed repetitive bending, sliding, and reannealing between pairs or small groups of outer doublet microtubules in the splayed axonemes from the *drc* mutants, similar to that seen in frayed doublets from WT axonemes (Aoyama and Kamiya, 2005). Thus, with the assembly of a stable axonemal base, the dynein motors and outer doublet microtubules are sufficient for producing simple, repetitive sliding-bending (Aoyama and Kamiya, 2005; Brokaw, 2009b), and, based on this study, repetitive motion between the outer doublet microtubules does not require the presence of the N-DRC.

Although simple, repetitive sliding-bending does not require the N-DRC, the connections provided by the N-DRC do appear to facilitate resistance to sliding along the length of the axoneme. This perspective is consistent with a distributor model in which the radial spokes (and central pair projections) activate subsets of dynein arms to exert force against the N-DRC linkages (Porter and Sale, 2000; Porter, 2012; Smith and Yang, 2004). In the absence of signals from the CP/RS complex, dynein activity is reduced, leading to decreased microtubule sliding and flagellar paralysis. Mutations in the N-DRC that weaken the connections between the outer doublet microtubules allow the dynein arms to generate microtubule sliding, even in the absence of signals from the CP/RS complex, and some form of motility is restored (Huang *et al.*, 1982). Thus the wild-type N-DRC functions to limit dynein arm activity indirectly along the length of the axoneme. Given that N-DRC subunits appear to be ubiquitous in motile axonemes (Table 3), the putative role of

the N-DRC in providing resistance to sliding should also be considered in the other models for regulating dynein cross-bridge activity and axonemal bending (see *Introduction*).

One unresolved question is how axonemes maintain their 9 + 2 organization in *drc*-mutant cells. We propose that that intact flagella of live cells contain other structures that contribute to axoneme integrity. These may include the capping structures at the flagellar tips that insert into the A-tubules of the outer doublets, connections between the outer doublets and the flagellar membrane, and/or other axonemal structures. Mutations have been identified in other organisms that lead to disorganization of the outer doublets (Dawe *et al.*, 2005; Baron *et al.*, 2007; Merveille *et al.*, 2011), but the precise location of the gene products is unresolved. The further characterization of the large collection of flagellar motility mutants available in *Chlamydomonas* may soon reveal the identity and location of the other components that contribute to axoneme integrity and coordinated motility.

The proximal axoneme is a relatively stable structure that provides resistance and contributes to motility

In most cilia and eukaryotic flagella, bends are initiated at the proximal end and then propagated distally. With notable exceptions (Holwill and McGregor, 1976; Woolley *et al.*, 2006), bends are not propagated in the reverse direction. In addition, the ability to initiate bending appears to be localized to a small region at the proximal axoneme (Goldstein, 1969), and ATP-induced reactivated movement of isolated axonemes also results in initiation and propagation of bends from the base (Gibbons and Gibbons, 1972; Shingyoji *et al.*, 1977). Furthermore, both experimental and theoretical evidence indicates the mechanical properties of the base of the axoneme are important for oscillatory bending (Goldstein, 1969; Fujimura and Okuno, 2006; Riedel-Kruse *et al.*, 2007; Mitchison and Mitchison, 2010; Woolley, 2010).

Our study of ATP-treated axonemes from *drc* mutants also reveals that the proximal axoneme is a relatively stable structure. We propose that the stability of the proximal axoneme prevents significant dislocation of adjacent doublet microtubules in the *drc* mutants. As a consequence, ATP addition results in splaying and reannealing of outer doublets rather than the linear sliding that leads to axoneme disintegration in protease-treated axonemes. We also conclude that the stability of the proximal axoneme is not based on known components of the N-DRC. Although the *drc* mutants examined in this study differ in the extent of their polypeptide deficiencies (Supplemental Table S4), we have no evidence to suggest that any of the subunits identified thus far vary along the length of the axoneme (Figure 2 and Supplemental Figure S4). However, we previously noted that the structural defects in *drc* mutants are more pronounced in medial/distal region of the axoneme than in the proximal region (Gardner *et al.*, 1994). The proximal region must therefore contain additional unique structures that link the outer doublets and maintain the integrity of the axoneme. However, with limited exceptions, we know little about the specialized structures (Witman *et al.*, 1978; Hoops and Witman, 1983; Bui *et al.*, 2012) and proteins (Mahjoub *et al.*, 2004; Iomini *et al.*, 2006; Yagi *et al.*, 2009) assembled at the base of the axoneme. Candidate components include minor inner-arm dyneins localized to the proximal axoneme (Yagi *et al.*, 2009; Bui *et al.*, 2012) and other interdoublet linkers of unknown composition (Witman *et al.*, 1978; Bui *et al.*, 2012; Lin *et al.*, 2012). We predict that these minor dyneins and/or uncharacterized interdoublet linkers in the proximal axoneme play an essential role in the initiation of axonemal bending and in providing additional resistance to dynein-driven sliding. Further study of the proximal region of the axoneme is required to identify these components and characterize their role in the organization of the axoneme and the regulation of ciliary and flagellar motility.

MATERIALS AND METHODS

Culture conditions, genetic analyses, and strain construction

The strains used in this study are listed in Supplemental Table S1. Cells were maintained on Tris-acetate phosphate medium but resuspended overnight in liquid minimal medium or 10 mM 4-(2-hydroxyethyl)-1-piperazineethanesulfonic acid (HEPES), pH 7.6, to facilitate flagellar assembly and mating.

A GFP-tagged version of PF2 was constructed by insertion of a codon-modified GFP into a 6.9-kb *Xma*I subclone (p9b11-X1.2) containing the complete WT *PF2* gene (Rupp and Porter, 2003). A *Bst*EII site was eliminated by site-directed mutagenesis of a CTG codon to a CTC codon in the pHisCrGFP plasmid (Fuhrmann *et al.*, 1999). The GFP tag was amplified using primers with *Bst*EII restriction sites, ligated into pGEM-T Easy (Promega, Madison, WI), and then digested and religated into a unique *Bst*EII site in the PF2 plasmid (Supplemental Table S2). Sequence analysis of the *PF2-GFP* subclone confirmed that the GFP tag was inserted into the 12th exon of the *PF2* gene in the proper orientation and reading frame. The GFP sequence is followed by 52 nucleotides (14 codons) encoding the last 13 amino acids of the PF2 polypeptide.

PF2-GFP rescued strains were generated by transforming *pf2-4* or *sup-pf3* with the *PF2-GFP* plasmid and the selectable marker pSI103 containing the *aphVIII* gene (Sizova *et al.*, 2001) and plating cells on Tris-acetate-phosphate medium containing 10 µg/ml paromomycin. GFP-positive cells were identified by fluorescence microscopy, and motility phenotypes were assessed by phase contrast microscopy. The *sup-pf4* strain was rescued by transformation with an ~7.4-kb *Bam*H1/*Xho*I subclone containing an HA-tagged *FAP155* gene derived from BAC 1i23. The stop codon in *FAP155* was mutated to an *Fse*I site, and the triple-HA tag was amplified using primers with *Fse*I sites (Supplemental Table S2).

Southern blots, PCR and sequence analysis, and library construction

Isolation of genomic DNA or total RNA, restriction enzyme digests, PCRs, and Southern blots were performed as previously described (Perrone *et al.*, 2000, 2003; Rupp *et al.*, 2001; Rupp and Porter, 2003). PCR primers were designed using the published sequence for the *PF2* gene (accession numbers AY309087 and AY3090088). DNA sequencing was performed by the Biomedical Genomics Center (St. Paul, MN) and analyzed using the Sequencher and MacVector software available through the Minnesota Supercomputing Institute (Minneapolis, MN). The predicted amino acid sequence (accession number AAP57169 or Q7XJ96) differs from the sequence reported by the *Chlamydomonas* genome project (XP_001697295) in the region corresponding to amino acid residues 152–197. Our predicted amino acid sequence was based on the direct sequencing of RT-PCR products (Rupp and Porter, 2003), whereas the genome project used gene-modeling programs to infer exon splice sites (Merchant *et al.*, 2007). Alignment of the predicted amino sequence with the most recent assembly of *Chlamydomonas* expressed sequence tags for *PF2* confirms our previously published sequence.

For identification of the site of the mutation in *sup-pf3*, genomic DNA was digested with *Sac*I, and restriction fragments ranging in size from 6 to 8 kb were used to create a mini–genomic library as described previously (Perrone *et al.*, 2000; Rupp and Porter, 2003). Colonies containing the modified ~7-kb *Sac*I fragment in *sup-pf3*

were identified by hybridization with a 1.2-kb *Nhe*I fragment corresponding to nucleotides 2146–3362 of the *PF2* gene. Sequence analysis of the subclone revealed the presence of a *TOC1* transposon in the middle of the *PF2* transcription unit (Supplemental Figure S2). The identification of a large genomic deletion in *sup-pf4* that includes the *FAP155* gene and two neighboring genes was previously described (Lin *et al.*, 2011).

Antibody production and characterization

A peptide corresponding to amino acid residues 87–108 (EERHQVEIKVYKQKKVKHLLYEH) of the *Chlamydomonas* PF2 sequence was synthesized by Research Genetics (Huntsville, AL), coupled to keyhole limpet hemocyanin, and used to immunize two rabbits. Polyclonal serum from both rabbits was pooled and purified over a peptide affinity column. A second antibody was raised against a fusion protein corresponding to amino acid residues 1–430 of the mouse GAS8 sequence (GenBank Accession number AA499529). A mouse cDNA clone (937316; Stratagene, Santa Clara, CA) was digested with *Nco*I and *Bam*HI and ligated into pET30a (Novagen, Gibbstown, NJ). The subclone was digested with *Bam*HI and *Hin*dIII, and a small synthetic *Bam*HI/*Hin*dIII linker containing two stop codons was ligated in-frame with the GAS8 sequence. Expression of the histidine (His)-tagged GAS8 fusion protein was induced overnight at 20°C, and soluble protein was purified on a Ni^{2+} column (Novagen), dialyzed into phosphate-buffered saline, and used to immunize three rabbits (Covance, Denver, PA). A second fusion protein was prepared by transferring the GAS8 sequence into pGEX-2T (Amersham) and purification of a glutathione *S*-transferase (GST)–GAS8 fusion protein on a glutathione–Sepharose column. The polyclonal antibody was blot affinity purified against either the His-tagged or the GST-tagged GAS8 fusion protein as described by Tang (1993). Alternatively, the GST-tagged GAS8 fusion protein was cross-linked to glutathione–Sepharose beads and used for column affinity purification of the antibody as described by the manufacturer. The affinity-purified antibodies were tested against blots of WT and *pf2-4* axonemes at a 1:1000 dilution. Some batches of affinity-purified antibodies demonstrated additional cross-reactivity against an ~100-kDa band in both WT and *pf2-4* axonemes. To reduce this background, the affinity-purified antibody was absorbed against methanol-extracted *pf2-4* cells or blots of *pf2-4* axonemes as previously described (Perrone *et al.*, 2003).

Peptides and/or fusion proteins from DRC4-associated polypeptides identified by coimmunoprecipitation and/or iTRAQ analysis were used to generate polyclonal antibodies in rabbits at Spring Valley Laboratories (Woodbine, MD) or Covance. The following peptides were synthesized and coupled to KLH via a C-terminal cysteine: FAP134 (AEINKGQYNGYFTQVRC), FAP50 (RRSTRKSKRGGDSKRLC), FAP169 (LPDANTWPTWGALRERC), FAP155 (ADEDYWRRRSQARWKNC), FAP200 (CASLFRDDYHTLLRAFRC), and FAP82 (EKRNPDTGEYPDFPDPC and GKPGTAGSKPGTADKKC). Peptides were coupled to SulfoLink (Pierce Chemical, Rockford, IL) for affinity purification of the resulting antisera. Fusion proteins corresponding to amino acid residues 853–1258 of FAP50, 311–500 of FAP82, and 1–573 of FAP250 were also generated using His, GST, and MBP tags. Antisera against FAP50 were generated with gel-purified 6xHis-FAP50 fusion protein and affinity purified against the FAP50-MBP fusion protein bound to an NHS agarose (ThermoFisher Scientific, Rockford, IL) column. Antisera against FAP250 were generated with gel-purified 6xHis-FAP250 fusion protein and blot affinity purified against the FAP250-GST protein. Antisera against FAP82 were generated with the FAP82-GST fusion protein purified from inclusion bodies.

Isolation of flagella and fractionation of the dynein regulatory complex

Flagella were isolated by pH shock or dibucaine treatment and demembranated using 0.1–0.5% IGEPAL CA-630 (Sigma Aldrich, St. Louis, MO) as previously described (Witman, 1986). Axonemes were resuspended in HMEEN (10 mM HEPES, pH 7.4, 5 mM $MgSO_4$, 1 mM ethylene glycol tetraacetic acid, 0.1 mM EDTA, 30 mM NaCl) plus 1 mM dithiothreitol (DTT) and 0.1 μg/ml protease inhibitors (leupeptin, aprotinin, pepstatin) and sequentially extracted with HMEEN containing 0.6 M NaCl, 0.2 M NaI, 0.4 M NaI, or 0.6 M NaI to identify optimal conditions for extraction of DRC4 in WT and different *drc* mutants. Extracts were dialyzed against HMEEN, clarified by centrifugation, and then fractionated on 5–20% sucrose density gradients. Sarkosyl-extracted protofilament ribbons were prepared as described in Norrander *et al.* (2000).

SDS–PAGE and Western blot analyses

Samples were analyzed on 5–15% polyacrylamide, 0–2.4 M glycerol gradient gels. Protein was transferred to Immobilon P (Millipore, Billerica, MA), and total protein on the blot was visualized with the reversible Blot FastStain (Chemicon, Temecula, CA) to ensure equal loading. Antibodies were diluted in Tropix I-Block (Applied Biosystems, Bedford, MA) at the concentrations indicated in Supplemental Table S3. Immunoreactive bands were detected with alkaline phosphatase–conjugated secondary antibodies and the Tropix chemiluminescent detection system.

Immunoprecipitation and mass spectrophotometry of DRC4-associated proteins

Immunoprecipitations were performed as described by Wargo *et al.* (2005) and Dymek and Smith (2007) with the following modifications. Isolated axonemes from WT, mutant, and rescued strains were extracted with 0.4-0.6 M NaI in HMEEN for 30 min on ice. Extracts were dialyzed against HMEEN or Na-low buffer (10 mM HEPES, pH 7.4, 5 mM $MgSO_4$, 1 mM DTT, 0.5 mM EDTA, and 30 mM NaCl) for a minimum of 2 h to overnight and clarified by centrifugation. From 40 to 200 μl of clarified extract (containing 40–300 μg of protein) were incubated for 3–24 h with Tris-buffered saline (TBS), 0.1% Tween, protein A or protein G beads, and 20–40 μg of one of the following antibodies: rabbit anti–CaM-IP2, rabbit anti-GAS8, Covance mouse anti-HA (clone 16B120), Roche rat anti-HA (clone 3F10; Roche, Indianapolis, IN), or rabbit anti-GFP (A11122; Invitrogen, Carlsbad, CA) for several hours. The beads were collected by centrifugation and washed four or five times with TBS/0.1% Tween and twice with TBS. Beads were boiled in sample buffer, and samples were loaded on 5–15% polyacrylamide gels for Western blotting and silver staining. Gels were stained with PROTSIL2-1KT (Sigma-Aldrich, St. Louis, MO) or SilverQuest (LC6070; Invitrogen).

Coomassie blue– or silver-stained bands from both experimental and control lanes were excised from the gel, destained, and subjected to cysteine reduction, alkylation and tryptic digestion on the Genomic Solution ProPrep robot (Ann Arbor, MI) in the Center for Mass Spectrometry and Proteomics at the University of Minnesota (St. Paul, MN) and processed as described in Andersen *et al.* (2010) with the following modifications. Tryptic peptides were extracted, dried down, and rehydrated in water/acetonitrile/formic acid (95:5:0.1). MS was performed on a linear ion trap (LTQ; Thermo Electron, San Jose, CA) using nanoscale microcapillary reversed-phase liquid chromatography electrospray ionization MS/MS. Peptide mixtures were autosampled on a Paradigm MS4 system (Michrom Bioresources, Auburn, CA). Samples were desalted and concentrated on a Paradigm Platinum Peptide Nanotrap (Michrom Bioresources)

precolumn (0.15 × 50 mm, 400-µl volume) and subsequently to a fused silica microcapillary column (75-µm internal diameter) packed in-house using a high-pressure helium bomb to a length of 13 cm with Magic C18AQ reversed-phase material on a flow splitter (Michrom Bioresources) at a flow rate of 250 nl/min. The samples were subjected to a 60-min (10–40% acetonitrile) gradient and directly eluted into the microcapillary column set to 2.0 kV. The LTQ was operated in the positive-ion mode using data-dependent acquisition methods initiated by a survey MS scan, which was followed by MS/MS (collision energy of 29%) on the four most abundant ions detected in the survey scan. The *m/z* values selected in the survey scan for MS/MS were dynamically excluded from further data-dependent MS/MS for a time of 30 s. The signal intensity threshold for an ion to be selected for MS/MS was set to a lower limit of 1000.

Sequence analysis and criteria for protein identification

Mass spectra were extracted and analyzed using BioWorks SeQuest Analysis Software package, SeQuest version SRF v. 27, revision 13 (ThermoFisher Scientific, San Jose, CA) against *Chlamydomonas* sequences at National Center for Biotechnology Information or the *Chlamydomonas* genome database (version 3.0; http://genome.jgi-psf.org/Chlre/Chlre3.home.html) for protein identification. The extracted data were also subjected to X! Tandem version 2007.01.01.1 searches within the Scaffold program (v_3_00_03; Proteome Software, Portland, OR). The data were searched with a fragment-ion mass tolerance of 1.00 Da and a parent-ion tolerance of 1.00 Da. Iodoacetamide derivative of cysteine was specified as a fixed modification and oxidation of methionine as a variable modification.

The Scaffold program was also used to validate MS/MS-based peptide and protein identifications. Peptide IDs were accepted if they could be established at >95.0% probability as specified by the Peptide Prophet algorithm (Keller *et al.*, 2002). Protein IDs were accepted if they could be established at >99.9% probability by the Protein Prophet algorithm (Nesvizhskii *et al.*, 2003) and contained at least three identified peptides. Proteins that contained similar peptides and could not be differentiated based on MS/MS analysis alone were grouped to satisfy the principles of parsimony. Any polypeptides detected in both experimental and control samples (e.g., tubulin) were considered contamination.

Preparation of samples for iTRAQ analysis

Axoneme samples were resuspended in 10 mM HEPES, pH 7.4, for estimation of the protein concentration and to remove salt, DTT, and protease inhibitors. After centrifugation at 16,000 rpm, the pellets were resuspended in 0.5 M triethylammonium bicarbonate, pH 8.5, at a concentration of 0.6–5.0 mg/ml. Proteins were denatured and reduced; cysteine residues were blocked with methylmethane thiosulfonate, and then samples were digested overnight at 37°C with trypsin. Aliquots of each sample (50 µg for the four-plex and 25 µg for the eight-plex) were reacted in duplicate with four-plex (114–117) or eight-plex (113–119, 121) iTRAQ labeling reagents (AB SCIEX, Foster City, CA). The labeled samples were combined, dried under vacuum, and purified with an MCX cartridge (Waters Corporation, Milford, MA) to remove excess trypsin, unreacted iTRAQ reagents, and buffer.

The labeled peptide mixture was first fractionated by strong-cation-exchange chromatography into 14 fractions, and then each fraction was subjected to capillary-LC with Magic C18AQ columns (Michrom Bioresources). The LC elutes were spotted onto MALDI targets in a 1232-spot format. MS data on all LC spots were acquired on 4800 MALDI-TOF/TOF analyzer (AB/MDS) with a 200-Hz repetition rate Nd:YAG laser. Full-scan MS spectra were acquired from *m/z* 800 to 4000. Data-dependent tandem MS settings included acquisition of the top 30 most intense ion signals per spot. Additional details were as previously reported (Akkina *et al.*, 2009).

Protein Pilot software version 3 (AB SCIEX) was used for data processing (Shilov *et al.*, 2007). Searches were performed against the *Chlamydomonas* version 3 database (translated from genomic sequences; http://genome.jgi-psf.org/Chlre3/Chlre3.home.html) plus common lab contaminant proteins (www.thegpm.org/crap/index.html). The quality of the protein identification was further assessed by the false-discovery-rate analysis (Tang *et al.*, 2008), and a 5% local false-discovery-rate threshold was set as the cut-off value for proteins subjected to quantification. Only those proteins identified with >95% confidence and whose WT/WT ratio varied <20% were considered further. A total of 252 proteins were detected in the four-plex experiment, and 188 proteins were detected in the eight-plex experiment.

The predicted amino acid sequences of proteins identified in the V3 database were compared with revised sequences in later releases of the *Chlamydomonas* genome project (V4, http://genome.jgi-psf.org/Chlre4/Chlre4.home.html; and V5, www.phytozome.net/search.php?show=text&org=Org_Creinhardtii_v5.3). Any ambiguous sequences were verified directly by RT-PCR of WT cDNA (Supplemental Table S2). The location of predicted protein domains was determined using the SMART program (available at http://smart.embl-heidelberg.de/).

Phase contrast and fluorescence microscopy

Swimming phenotypes were assessed by phase contrast microscopy using a 40× objective and 1.6× eyepiece (Rupp and Porter, 2003). The distribution of DRC4-GFP in live cells was analyzed using either a Zeiss Axioskop (Carl Zeiss, Jena, Germany) as described later or a Nikon Eclipse E800 photomicroscope (Nikon, Melville, NY) using a 100×/1.3 numerical aperture (NA) Plan Apo objective, a Photometrics Cascade 512B camera (Photometric, Tucson, AZ), and the ImagePro Plus software package available at the University Imaging Center (St. Paul, MN). Live cells were immobilized with 1% low–melting point agarose and/or allowed to adhere to polyethanolamine-treated coverslips before imaging. Image stacks were collected using *z*-steps of 0.339 µm. For the image shown in Figure 2A, sections 11–21 were deconvolved using ImagePro Plus 6.2 Sharp Stack and then used to make a maximum-intensity projection.

Because the DRC4-GFP signal bleaches quickly, most cells were fixed using ice-cold methanol (Sanders and Salisbury, 1995) and stained for immunofluorescence using a mouse monoclonal antibody to GFP (Molecular Probes) or a rat monoclonal antibody to HA (clone 3F10; Roche) and Alexa Fluor–488 conjugated secondary antibodies (Molecular Probes) as described by Mueller *et al.* (2005). Slides were sealed using either SlowFade or Prolong Gold mounting medium (Invitrogen Life Technologies, Grand Island, NY). Images were collected on a Zeiss Axioscop equipped with differential interference contrast (DIC) and wide-field fluorescence optics using a 100×/1.3NA Plan Neofluar objective, a CoolSNAP-ES monochrome charge-coupled device camera (Photometrics), and the MetaMorph Software package, version 7.1.7.0 (Molecular Devices, Downington, PA). Selected images were cropped, rotated, and labeled in Photoshop (Adobe, San Jose, CA).

Analysis of microtubule sliding and splaying in isolated axonemes

Microtubule sliding and splaying was measured as previously described (Okagaki and Kamiya, 1986; Habermacher and Sale, 1996) with the following modifications. Briefly, isolated flagella were

resuspended in buffer without protease inhibitors and demembranated with buffer containing 0.5% Nonidet P-40 in 10 mM HEPES, pH 7.4, 5 mM $MgSO_4$, 1 mM DTT, 0.5 mM EDTA, 1% polyethylene glycol (20,000 molecular weight), and 25 mM potassium acetate. The unsonicated, full-length axonemes were added to a perfusion chamber, constructed using double-stick tape as spacers between the coverslip and slide, and permitted to adhere to the glass surfaces, and microtubule sliding/splaying was initiated by the addition of buffer containing 0.1 mM ATP or 0.1 mM ATP and subtilisin A type VIII protease at 5 μg/ml (Sigma-Aldrich). Assays of microtubule sliding disintegration often use short axoneme fragments obtained by sonication (e.g., Kubo *et al.*, 2012), but we found that it was essential to use unsonicated, full-length axonemes and lower concentrations of ATP to detect the splaying phenomenon. Images were recorded using a Zeiss Axiovert 35 microscope equipped with dark-field optics, a Zeiss 40× Plan-Apo lens, and a silicon intensified camera (VE-1000; Dage-MTI, Michigan City, IN). The video images were converted to a digital format using Labview 7.1 software (National Instruments, Austin, TX), and sliding or splaying was determined manually by counting multiple fields of axonemes at ~15 s after motility was initiated. All axonemes observed within a field were scored as intact, splayed (held together at the proximal end), or disrupted by linear sliding. At least 70 axonemes were counted per treatment in each experiment.

ACKNOWLEDGMENTS

We thank Lorraine Anderson, LeeAnn Higgins, Todd Markowski, and Bruce Witthun of the Center for Mass Spectrometry and Computational Proteomics at the University of Minnesota for assistance with iTRAQ labeling, mass spectrometry, and spectral counting. The Center is supported by multiple grants, including National Science Foundation Major Research Instrumentation Grants 9871237 and NSF-DBI-0215759 as described at www.cbs.umn.edu/msp/about. We also acknowledge the University of Minnesota Supercomputing Institute for software support and data storage and Mark Sanders and the University Imaging Center for assistance with live-cell imaging. We also thank Matt Laudon and the *Chlamydomonas* Genetics Center (University of Minnesota) for strains. Richard Linck (University of Minnesota), Mark Sanders (University of Minnesota), Ritsu Kamiya (University of Tokyo, Tokyo, Japan), Toshiki Yagi (Kyoto University, Kyoto, Japan), Pinfen Yang (Marquette University, Milwaukee, WI), Elizabeth Smith (Dartmouth College, Hanover, NH), and Gianni Piperno (Mount Sinai School of Medicine, New York, NY) generously supplied antibodies as listed in Supplemental Table S3. Preliminary reports of this work were presented at American Society for Cell Biology meetings in 2006 and 2010. This work was supported by National Institutes of Health grants to M.E.P. (GM-055667) and W.S.S. (GM-051173). K.V.M. was supported in part by an American Heart Association Pre-Doctoral Fellowship and a University of Minnesota Graduate School Fellowship, and M.E.P. was recipient of University of Minnesota Graduate School Grant 20828.

REFERENCES

Ahmed NT, Gao C, Lucker BF, Cole DG, Mitchell DR (2008). ODA16 aids axonemal outer row dynein assembly through an interaction with the intraflagellar transport machinery. J Cell Biol 183, 313–322.

Akkina SK, Zhang Y, Nelsestuen GL, Oetting WS, Ibrahlm HN (2009). Temporal stability of the urinary proteome after kidney transplant: more sensitive than protein composition? J Proteome Res 8, 94–103.

Andersen JD, Boylan KL, Xue FS, Anderson LB, Witthuhn BA, Markowski TW, Higgins L, Skubitz AP (2010). Identification of candidate biomarkers in ovarian cancer serum by depletion of highly abundant proteins and differential in-gel electrophoresis. Electrophoresis 31, 599–610.

Aoyama S, Kamiya R (2005). Cyclical interactions between two outer doublet microtubules in split flagellar axonemes. Biophys J 89, 3261–3268.

Armbrust EV *et al.* (2004). The genome of the diatom *Thalassiosira pseudonana*: ecology, evolution, and metabolism. Science 306, 79–86.

Barber CF, Heuser T, Carbajal-Gonzalez BI, Botchkarev VV Jr, Nicastro D (2012). Three-dimensional structure of the radial spokes reveals heterogeneity and interactions with dyneins in *Chlamydomonas* flagella. Mol Biol Cell 23, 111–120.

Baron DM, Ralston KS, Kabututu ZP, Hill KL (2007). Functional genomics in *Trypanosoma brucei* identifies evolutionarily conserved components of motile flagella. J Cell Sci 120, 478–491.

Bekker JM, Colantonio JR, Stephens AD, Clarke WT, King SJ, Hill KL, Crosbie RH (2007). Direct interaction of Gas11 with microtubules: implications for the dynein regulatory complex. Cell Motil Cytoskeleton 64, 461–473.

Bozkurt HH, Woolley DM (1993). Morphology of nexin links in relation to interdoublet sliding in the sperm flagellum. Cell Motil Cytoskeleton 24, 109–118.

Brokaw CJ (2009a). Thinking about flagellar oscillation. Cell Motil Cytoskeleton 66, 425–436.

Brokaw CJ (2009b). Simulation of cyclic dynein-driven sliding, splitting, and reassociation in an outer doublet pair. Biophys J 97, 2939–2947.

Brokaw CJ, Kamiya R (1987). Bending patterns of *Chlamydomonas* flagella: IV. Mutants with defects in inner and outer dynein arms indicate differences in dynein arm function. Cell Motil Cytoskeleton 8, 68–75.

Brokaw CJ, Luck DJ (1985). Bending patterns of *Chlamydomonas* flagella: III. A radial spoke head deficient mutant and a central pair deficient mutant. Cell Motil 5, 195–208.

Brokaw CJ, Luck DJ, Huang B (1982). Analysis of the movement of *Chlamydomonas* flagella: the function of the radial-spoke system is revealed by comparison of wild-type and mutant flagella. J Cell Biol 92, 722–732.

Bui KH, Sakakibara H, Movassagh T, Oiwa K, Ishikawa T (2009). Asymmetry of inner dynein arms and inter-doublet links in *Chlamydomonas* flagella. J Cell Biol 186, 437–446.

Bui KH, Yagi T, Yamamoto R, Kamiya R, Ishikawa T (2012). Polarity and asymmetry in the arrangement of dynein and related structures in the *Chlamydomonas* axoneme. J Cell Biol 198, 913–925.

Colantonio JR, Vermot J, Wu D, Langenbacher AD, Fraser S, Chen JN, Hill KL (2009). The dynein regulatory complex is required for ciliary motility and otolith biogenesis in the inner ear. Nature 457, 205–209.

Cole DG, Diener DR, Himelblau AL, Beech PL, Fuster JC, Rosenbaum JL (1998). *Chlamydomonas* kinesin-II-dependent intraflagellar transport (IFT): IFT particles contain proteins required for ciliary assembly in *Caenorhabditis elegans* sensory neurons. J Cell Biol 141, 993–1008.

Dawe HR, Farr H, Portman N, Shaw MK, Gull K (2005). The Parkin co-regulated gene product, PACRG, is an evolutionarily conserved axonemal protein that functions in outer-doublet microtubule morphogenesis. J Cell Sci 118, 5421–5430.

Day A, Rochaix JD (1991). A transposon with an unusual LTR arrangement from Chlamydomonas reinhardtii contains an internal tandem array of 76 bp repeats. Nucleic Acids Res 19, 1259–1266.

Drummond IA (2012). Cilia functions in development. Curr Opin Cell Biol 24, 24–30.

Dymek EE, Heuser T, Nicastro D, Smith EF (2011). The CSC is required for complete radial spoke assembly and wild-type ciliary motility. Mol Biol Cell 22, 2520–2531.

Dymek EE, Smith EF (2007). A conserved CaM- and radial spoke associated complex mediates regulation of flagellar dynein activity. J Cell Biol 179, 515–526.

Fliegauf M, Benzing T, Omran H (2007). When cilia go bad: cilia defects and ciliopathies. Nat Rev Mol Cell Biol 8, 880–893.

Fox LA, Sale WS (1987). Direction of force generated by the inner row of dynein arms on flagellar microtubules. J Cell Biol 105, 1781–1787.

Fuhrmann M, Oertel W, Hegemann P (1999). A synthetic gene coding for the green fluorescent protein (GFP) is a versatile reporter in *Chlamydomonas reinhardtii*. Plant J 19, 353–361.

Fujimura M, Okuno M (2006). Requirement of the fixed end for spontaneous beating in flagella. J Exp Biol 209, 1336–1343.

Gardner LC, O'Toole E, Perrone CA, Giddings T, Porter ME (1994). Components of a "dynein regulatory complex" are located at the junction between the radial spokes and the dynein arms in *Chlamydomonas* flagella. J Cell Biol 127, 1311–1325.

Gibbons BH, Gibbons IR (1972). Flagellar movement and ATPase activity in sea urchin sperm extracted with Triton X-100. J Cell Biol 54, 75–97.

Gibbons IR (1963). Studies on the protein components of cilia from *Tetrahymena pyriformis*. Proc Natl Acad Sci USA 50, 1002–1010.
Gibbons IR (1965). Chemical dissection of cilia. Arch Biol (Liege) 76, 317–352.
Gluenz E, Hoog JL, Smith AE, Dawe HR, Shaw MK, Gull K (2010). Beyond 9+0: noncanonical axoneme structures characterize sensory cilia from protists to humans. FASEB J 24, 3117–3121.
Goldstein SF (1969). Irradiation of sperm tails by laser microbeam. J Exp Biol 51, 431–441.
Gupta A, Diener DR, Sivadas P, Rosenbaum JL, Yang P (2012). The versatile molecular complex component LC8 promotes several distinct steps of flagellar assembly. J Cell Biol 198, 115–126.
Habermacher G, Sale WS (1996). Regulation of flagellar dynein by an axonemal type-1 phosphatase in *Chlamydomonas*. J Cell Sci 109 Pt 7, 1899–1907.
Hayashi S, Shingyoji C (2008). Mechanism of flagellar oscillation-bending-induced switching of dynein activity in elastase-treated axonemes of sea urchin sperm. J Cell Sci 121, 2833–2843.
Heuser T, Barber CF, Lin J, Krell J, Rebesco M, Porter ME, Nicastro D (2012b). Cryoelectron tomography reveals doublet-specific structures and unique interactions in the I1 dynein. Proc Natl Acad Sci USA 109, E2067–E2076.
Heuser T, Dymek EE, Lin J, Smith EF, Nicastro D (2012a). The CSC connects three major axonemal complexes involved in dynein regulation. Mol Biol Cell 23, 3143–3155.
Heuser T, Raytchev M, Krell J, Porter ME, Nicastro D (2009). The dynein regulatory complex is the nexin link and a major regulatory node in cilia and flagella. J Cell Biol 187, 921–933.
Hildebrandt F, Benzing T, Katsanis N (2011). Ciliopathies. N Engl J Med 364, 1533–1543.
Hill KL, Hutchings NR, Grandgenett PM, Donelson JE (2000). T lymphocyte-triggering factor of African trypanosomes is associated with the flagellar fraction of the cytoskeleton and represents a new family of proteins that are present in several divergent eukaryotes. J Biol Chem 275, 39369–39378.
Hodges ME, Wickstead B, Gull K, Langdale JA (2011). Conservation of ciliary proteins in plants with no cilia. BMC Plant Biol 11, 185.
Holwill MEJ, McGregor JL (1976). Effects of calcium on flagellar movement in the trypanosome *Crithidia oncopelti*. J Exp Biol 65, 222–242.
Hoops HJ, Witman GB (1983). Outer doublet heterogeneity reveals structural polarity related to beat direction in *Chlamydomonas* flagella. J Cell Biol 97, 902–908.
Hou Y, Qin H, Follit JA, Pazour GJ, Rosenbaum JL, Witman GB (2007). Functional analysis of an individual IFT protein: IFT46 is required for transport of outer dynein arms into flagella. J Cell Biol 176, 653–665.
Huang B, Ramanis Z, Luck DJ (1982). Suppressor mutations in *Chlamydomonas* reveal a regulatory mechanism for flagellar function. Cell 28, 115–124.
Ikeda K, Brown JA, Yagi T, Norrander JM, Hirono M, Eccleston E, Kamiya R, Linck RW (2003). Rib72, a conserved protein associated with the ribbon compartment of flagellar A-microtubules and potentially involved in the linkage between outer doublet microtubules. J Biol Chem 278, 7725–7734.
Ikeda K, Ikeda T, Morikawa K, Kamiya R (2007). Axonemal localization of *Chlamydomonas* PACRG, a homologue of the human Parkin-coregulated gene product. Cell Motil Cytoskeleton 64, 814–821.
Iomini C, Li L, Mo W, Dutcher SK, Piperno G (2006). Two flagellar genes, *AGG2* and *AGG3*, mediate orientation to light in *Chlamydomonas*. Curr Biol 16, 1147–1153.
Ishikawa H, Thompson J, Yates JR 3rd, Marshall WF (2012). Proteomic analysis of mammalian primary cilia. Curr Biol 22, 414–419.
Johnson KA, Rosenbaum JL (1992). Polarity of flagellar assembly in *Chlamydomonas*. J Cell Biol 119, 1605–1611.
Kabututu ZP, Thayer M, Melehani JH, Hill KL (2010). CMF70 is a subunit of the dynein regulatory complex. J Cell Sci 123, 3587–3595.
Keller A, Nesvizhskii AI, Kolker E, Aebersold R (2002). Empirical statistical model to estimate the accuracy of peptide identifications made by MS/MS and database search. Anal Chem 74, 5383–5392.
Kubo T, Yagi T, Kamiya R (2012). Tubulin polyglutamylation regulates flagellar motility by controlling a specific inner-arm dynein that interacts with the dynein regulatory complex. Cytoskeleton (Hoboken) 69, 1059–1068.
Kubo T, Yanagisawa HA, Yagi T, Hirono M, Kamiya R (2010). Tubulin polyglutamylation regulates axonemal motility by modulating activities of inner-arm dyneins. Curr Biol 20, 441–445.
Lechtreck KF, Johnson EC, Sakai T, Cochran D, Ballif BA, Rush J, Pazour G, Ikebe M, Witman GB (2009a). HA-tagging of putative flagellar proteins in *Chlamydomonas reinhardtii* identifies a novel protein of intraflagellar transport complex B. Cell Motil Cytoskeleton 66, 469–482.
Lechtreck KF, Johnson EC, Sakai T, Cochran D, Ballif BA, Rush J, Pazour GJ, Ikebe M, Witman GB (2009b). The *Chlamydomonas reinhardtii* BBSome is an IFT cargo required for export of specific signaling proteins from flagella. J Cell Biol 187, 1117–1132.
Lee L (2011). Mechanisms of mammalian ciliary motility: Insights from primary ciliary dyskinesia genetics. Gene 473, 57–66.
Li JB *et al.* (2004). Comparative genomics identifies a flagellar and basal body proteome that includes the BBS5 human disease gene. Cell 117, 541–552.
Lin J, Heuser T, Song K, Fu X, Nicastro D (2012). One of the nine doublet microtubules of eukaryotic flagella exhibits unique and partially conserved structures. PLoS One 7, e46494.
Lin J, Tritschler D, Song K, Barber CF, Cobb JS, Porter ME, Nicastro D (2011). Building blocks of the nexin-dynein regulatory complex in *Chlamydomonas* flagella. J Biol Chem 286, 29175–29191.
Linck RW (1973). Chemical and structural differences between cilia and flagella from the lamellibranch mollusc, *Aequipecten irradians*. J Cell Sci 12, 951–981.
Lindemann CB (2011). Experimental evidence for the geometric clutch hypothesis. Curr Top Dev Biol 95, 1–31.
Lindemann CB, Lesich KA (2010). Flagellar and ciliary beating: the proven and the possible. J Cell Sci 123, 519–528.
Lindemann CB, Macauley LJ, Lesich KA (2005). The counterbend phenomenon in dynein-disabled rat sperm flagella and what it reveals about the interdoublet elasticity. Biophys J 89, 1165–1174.
Lindemann CB, Mitchell DR (2007). Evidence for axonemal distortion during the flagellar beat of *Chlamydomonas*. Cell Motil Cytoskeleton 64, 580–589.
Mahjoub MR, Qasim Rasi M, Quarmby LM (2004). A NIMA-related kinase, Fa2p, localizes to a novel site in the proximal cilia of *Chlamydomonas* and mouse kidney cells. Mol Biol Cell 15, 5172–5186.
Mahoney DW, Therneau TM, Heppelmann CJ, Higgins L, Benson LM, Zenka RM, Jagtap P, Nelsestuen GL, Bergen HR, Oberg AL (2011). Relative quantification: characterization of bias, variability and fold changes in mass spectrometry data from iTRAQ-labeled peptides. J Proteome Res 10, 4325–4333.
Mastronarde DN, O'Toole ET, McDonald KL, McIntosh JR, Porter ME (1992). Arrangement of inner dynein arms in wild-type and mutant flagella of *Chlamydomonas*. J Cell Biol 118, 1145–1162.
Merchant SS *et al.* (2007). The *Chlamydomonas* genome reveals the evolution of key animal and plant functions. Science 318, 245–250.
Merveille AC *et al.* (2011). CCDC39 is required for assembly of inner dynein arms and the dynein regulatory complex and for normal ciliary motility in humans and dogs. Nat Genet 43, 72–78.
Mueller J, Perrone CA, Bower R, Cole DG, Porter ME (2005). The *FLA3* KAP subunit is required for localization of kinesin-2 to the site of flagellar assembly and processive anterograde intraflagellar transport. Mol Biol Cell 16, 1341–1354.
Minoura I, Yagi T, Kamiya R (1999). Direct measurement of inter-doublet elasticity in flagellar axonemes. Cell Struct Funct 24, 27–33.
Mitchell DR, Sale WS (1999). Characterization of a *Chlamydomonas* insertional mutant that disrupts flagellar central pair microtubule-associated structures. J Cell Biol 144, 293–304.
Mitchison TJ, Mitchison HM (2010). Cell biology: how cilia beat. Nature 463, 308–309.
Mizuno N, Taschner M, Engel BD, Lorentzen E (2012). Structural studies of ciliary components. J Mol Biol 422, 163–180.
Morita Y, Shingyoji C (2004). Effects of imposed bending on microtubule sliding in sperm flagella. Curr Biol 14, 2113–2118.
Nesvizhskii AI, Keller A, Kolker E, Aebersold R (2003). A statistical model for identifying proteins by tandem mass spectrometry. Anal Chem 75, 4646–4658.
Nishimura N, Araki K, Shinahara W, Nakano Y, Nishimura K, Higashio H, Sasaki T (2008). Interaction of Rab3B with microtubule-binding protein Gas8 in NIH 3T3 cells. Arch Biochem Biophys 474, 136–142.
Norrander JM, deCathelineau AM, Brown JA, Porter ME, Linck RW (2000). The Rib43a protein is associated with forming the specialized protofilament ribbons of flagellar microtubules in *Chlamydomonas*. Mol Biol Cell 11, 201–215.
Okagaki T, Kamiya R (1986). Microtubule sliding in mutant *Chlamydomonas* devoid of outer dynein arms. J Cell Biol 103, 1895–1902.
Pazour GJ, Agrin N, Leszyk J, Witman GB (2005). Proteomic analysis of a eukaryotic cilium. J Cell Biol 170, 103–113.

Perrone CA, Myster SH, Bower R, O'Toole ET, Porter ME (2000). Insights into the structural organization of the I1 inner arm dynein from a domain analysis of the 1beta dynein heavy chain. Mol Biol Cell 11, 2297–2313.

Perrone CA, Tritschler D, Taulman P, Bower R, Yoder BK, Porter ME (2003). A novel dynein light intermediate chain colocalizes with the retrograde motor for intraflagellar transport at sites of axoneme assembly in *Chlamydomonas* and mammalian cells. Mol Biol Cell 14, 2041–2056.

Pigino G, Bui KH, Maheshwari A, Lupetti P, Diener D, Ishikawa T (2011). Cryoelectron tomography of radial spokes in cilia and flagella. J Cell Biol 195, 673–687.

Pigino G, Maheshwari A, Bui KH, Shingyoji C, Kamimura S, Ishikawa T (2012). Comparative structural analysis of eukaryotic flagella and cilia from *Chlamydomonas, Tetrahymena,* and sea urchins. J Struct Biol 178, 199–206.

Piperno G (1995). Regulation of dynein activity within *Chlamydomonas* flagella. Cell Motil Cytoskeleton 32, 103–105.

Piperno G, Luck DJL (1979). Axonemal adenosine triphosphatases from flagella of *Chlamydomonas reinhardtii*. Purification of two dyneins. J Biol Chem 254, 3084–3090.

Piperno G, Mead K, LeDizet M, Moscatelli A (1994). Mutations in the "dynein regulatory complex" alter the ATP-insensitive binding sites for inner arm dyneins in *Chlamydomonas* axonemes. J Cell Biol 125, 1109–1117.

Piperno G, Mead K, Shestak W (1992). The inner dynein arms I2 interact with a "dynein regulatory complex" in *Chlamydomonas* flagella. J Cell Biol 118, 1455–1463.

Porter ME (2012). King SM (2012). Flagellar motility and the dynein regulatory complex. In: Dyneins: Structure, Biology, and Disease, Waltham, MA: Elsevier, 337–365.

Porter ME, Knott JA, Myster SH, Farlow SJ (1996). The dynein gene family in *Chlamydomonas reinhardtii*. Genetics 144, 569–585.

Porter ME, Sale WS (2000). The 9 + 2 axoneme anchors multiple inner arm dyneins and a network of kinases and phosphatases that control motility. J Cell Biol 151, F37–F42.

Portman N, Lacomble S, Thomas B, McKean PG, Gull K (2009). Combining RNA interference mutants and comparative proteomics to identify protein components and dependences in a eukaryotic flagellum. J Biol Chem 284, 5610–5619.

Qin H, Diener DR, Geimer S, Cole DG, Rosenbaum JL (2004). Intraflagellar transport (IFT) cargo: IFT transports flagellar precursors to the tip and turnover products to the cell body. J Cell Biol 164, 255–266.

Ralston KS, Hill KL (2006). Trypanin, a component of the flagellar dynein regulatory complex, is essential in bloodstream form African trypanosomes. PLoS pathogens 2, e101.

Rensing SA *et al*. (2008). The *Physcomitrella* genome reveals evolutionary insights into the conquest of land by plants. Science 319, 64–69.

Riedel-Kruse IH, Hilfinger A, Howard J, Julicher F (2007). How molecular motors shape the flagellar beat. HFSP J 1, 192–208.

Rupp G, O'Toole E, Porter ME (2001). The *Chlamydomonas PF6* locus encodes a large alanine/proline-rich polypeptide that is required for assembly of a central pair projection and regulates flagellar motility. Mol Biol Cell 12, 739–751.

Rupp G, Porter ME (2003). A subunit of the dynein regulatory complex in *Chlamydomonas* is a homologue of a growth arrest-specific gene product. J Cell Biol 162, 47–57.

Rushforth AM, Anderson P (1996). Splicing removes the *Caenorhabditis elegans* transposon Tc1 from most mutant pre-mRNAs. Mol Cell Biol 16, 422–429.

Sale WS, Satir P (1977). Direction of active sliding of microtubules in *Tetrahymena* cilia. Proc Natl Acad Sci USA 74, 2045–2049.

Sanders MA, Salisbury JL (1995). Immunofluorescence microscopy of cilia and flagella. Methods Cell Biol 47, 163–169.

Satir P, Matsuoka T (1989). Splitting the ciliary axoneme: implications for a "switch-point" model of dynein arm activity in ciliary motion. Cell Motil Cytoskeleton 14, 345–358.

Shilov IV, Seymour SL, Patel AA, Loboda A, Tang WH, Keating SP, Hunter CL, Nuwaysir LM, Schaeffer DA (2007). The paragon algorithm, a next generation search engine that uses sequence temperature values and feature probabilities to identify peptides from tandem mass spectra. Mol Cell Proteomics 6, 1638–1655.

Shingyoji C, Murakami A, Takahashi K (1977). Local reactivation of Triton-extracted flagella by iontophoretic application of ATP. Nature 265, 269–270.

Sizova I, Fuhrmann M, Hegemann P (2001). A *Streptomyces rimosus aphVIII* gene coding for a new type phosphotransferase provides stable antibiotic resistance to *Chlamydomonas reinhardtii*. Gene 277, 221–229.

Smith EF, Sale WS (1992). Regulation of dynein-driven microtubule sliding by the radial spokes in flagella. Science 257, 1557–1559.

Smith EF, Yang P (2004). The radial spokes and central apparatus: mechano-chemical transducers that regulate flagellar motility. Cell Motil Cytoskeleton 57, 8–17.

Snider J, Houry WA (2008). AAA+ proteins: diversity in function, similarity in structure. Biochem Soc Trans 36, 72–77.

Stephens RE (1970). Thermal fractionation of outer fiber doublet microtubules into A- and B-subfiber components. A- and B-tubulin. J Mol Biol 47, 353–363.

Stephens RE, Oleszko-Szuts S, Linck RW (1989). Retention of ciliary ninefold structure after removal of microtubules. J Cell Sci 92 Pt 3, 391–402.

Summers KE, Gibbons IR (1971). Adenosine triphosphate-induced sliding of tubules in trypsin-treated flagella of sea-urchin sperm. Proc Natl Acad Sci USA 68, 3092–3096.

Summers KE, Gibbons IR (1973). Effects of trypsin digestion on flagellar structures and their relationship to motility. J Cell Biol 58, 618–629.

Tang WH, Shilov IV, Seymour SL (2008). Nonlinear fitting method for determining local false discovery rates from decoy database searches. J Proteome Res 7, 3661–3667.

Tang WJ (1993). Blot-affinity purification of antibodies. Methods Cell Biol 37, 95–104.

Wais-Steider J, Satir P (1979). Effect of vanadate on gill cilia: switching mechanism in ciliary beat. J Supramol Struct 11, 339–347.

Wargo MJ, Dymek EE, Smith EF (2005). Calmodulin and PF6 are components of a complex that localizes to the C1 microtubule of the flagellar central apparatus. J Cell Sci 118, 4655–4665.

Wirschell M *et al*. (2013). The nexin-dynein regulatory complex subunit DRC1 is essential for motile cilia function in algae and humans. Nat Genet 45, 262–268.

Wirschell M, Yamamoto R, Alford L, Gokhale A, Gaillard A, Sale WS (2011). Regulation of ciliary motility: conserved protein kinases and phosphatases are targeted and anchored in the ciliary axoneme. Arch Biochem Biophys 510, 93–100.

Wirschell M, Zhao F, Yang C, Yang P, Diener D, Gaillard A, Rosenbaum JL, Sale WS (2008). Building a radial spoke: flagellar radial spoke protein 3 (RSP3) is a dimer. Cell Motil Cytoskeleton 65, 238–248.

Witman GB (1986). Isolation of *Chlamydomonas* flagella and flagellar axonemes. Methods Enzymol 134, 280–290.

Witman GB, Plummer J, Sander G (1978). *Chlamydomonas* flagellar mutants lacking radial spokes and central tubules. Structure, composition, and function of specific axonemal components. J Cell Biol 76, 729–747.

Woolley D, Gadelha C, Gull K (2006). Evidence for a sliding-resistance at the tip of the trypanosome flagellum. Cell Motil Cytoskeleton 63, 741–746.

Woolley DM (2010). Flagellar oscillation: a commentary on proposed mechanisms. Biol Rev Camb Philos Soc 85, 453–470.

Worden AZ *et al*. (2009). Green evolution and dynamic adaptations revealed by genomes of the marine picoeukaryotes *Micromonas*. Science 324, 268–272.

Yagi T, Uematsu K, Liu Z, Kamiya R (2009). Identification of dyneins that localize exclusively to the proximal portion of *Chlamydomonas* flagella. J Cell Sci 122, 1306–1314.

Yang P, Diener DR, Rosenbaum JL, Sale WS (2001). Localization of calmodulin and dynein light chain LC8 in flagellar radial spokes. J Cell Biol 153, 1315–1326.

Yang P, Smith EF (2009). The flagellar radial spokes. In: The *Chlamydomonas* Sourcebook, ed. GB Witman, San Diego, CA: Elsevier, 3, 209–234.

Yang Y *et al*. (2011). Regulation of flagellar motility by the conserved flagellar protein CG34110/Ccdc135/FAP50. Mol Biol Cell 22, 976–987.

Zariwala MA, Omran H, Ferkol TW (2011). The emerging genetics of primary ciliary dyskinesia. Proc Am Thorac Soc 8, 430–433.

Zhang D, Aravind L (2012). Novel transglutaminase-like peptidase and C2 domains elucidate the structure, biogenesis and evolution of the ciliary compartment. Cell Cycle 11, 3861–3875.

Zhu W, Smith JW, Huang CM (2010). Mass spectrometry-based label-free quantitative proteomics. J Biomed Biotechnol 2010, 840518.